

Spatiotemporal Reconnaissance Investigation of Phreatophyte Vegetation Vigor for Selected Hydrographic Areas in Nevada

**Justin L. Huntington
Blake Minor
Matthew Bromley
Charles Morton**

May 2018



Paradise Valley, NV

Prepared by

Division of Hydrologic Sciences, Desert Research Institute, Reno, NV

Prepared for

The Nature Conservancy

THIS PAGE INTENTIONALLY LEFT BLANK

CONTENTS

INTRODUCTION.....	1
OBJECTIVES	1
BACKGROUND & PREVIOUS WORK	1
APPROACH	3
METHODS	5
Landsat Image Processing.....	5
Groundwater Level Database	6
Site Visits, GIS, and Photograph Database	7
Gridded Climate Data Processing.....	7
RESULTS	8
Kings River Valley (HA 30A).....	8
Quinn River Valley (HA 33A – Orovada Subarea).....	14
Upper Reese River Valley (HA 56).....	18
Paradise Valley (HA 69).....	22
Grass Valley (HA 71).....	25
Edwards Creek Valley (HA 133).....	28
DISCUSSION and CONCLUSIONS.....	28
FUTURE WORK	31
REFERENCES.....	33
APPENDIX 1 – Select Site Photographs and Well Hydrographs.....	37
Appendix 1-1. Kings River Valley (HA 30A) Close-up, Site Photographs, Well Hydrographs, and AOI EVI-PPT Graphs for Eastern Part of the Valley.....	37
Appendix 1-2. Kings River Valley (HA 30A) Close-up, Site Photographs, Well Hydrographs, and AOI EVI-PPT Graphs for South-Eastern part of the Valley.....	39
Appendix 1-3. Quinn River Valley (HA 33A) Close-up, Site Photograph and Well Hydrographs for North-Central part of the Valley	41
Appendix 1-4. Quinn River Valley (HA 33A) Close-up, Site Photographs, Well Hydrographs, and AOI EVI-PPT Graph for North-Western part of the Valley.....	43
Appendix 1-5. Quinn River Valley (HA 33A) Close-up and Hydrographs for Wells along the Quinn River.....	45

Appendix 1-6. Upper Reese River Valley (HA 56) Close-up, Site Photographs, and AOI EVI-PPT Graph for Southern Part of the Valley	47
Appendix 1-7. Upper Reese River Valley (HA 56) Close-up and Site Photographs for the Eastern Part of the Valley.....	49
Appendix 1-8. Upper Reese River Valley (HA 56) Close-up, Site Photographs, Well Hydrographs, and AOI EVI-PPT Graphs for Western Part of the Valley	50
Appendix 1-9. Paradise Valley (HA 69) Close-up, Site Photographs, Well Hydrographs, and AOI EVI-PPT Graph for South-Eastern Part of the Valley.....	53
Appendix 1-10. Paradise Valley (HA 69) Close-up, Site Photographs, and Well Hydrograph for Southern Part of the Valley	55
Appendix 1-11. Paradise Valley (HA 69) Close-up, Site Photographs, Well Hydrographs, and AOI EVI-PPT Graph for North-Central Part of the Valley	57
Appendix 1-12. Grass Valley (HA 71) Close-up, Site Photographs, Well Hydrographs, and AOI EVI-PPT Graphs for Central Part of the Valley	59
Appendix 1-13. Grass Valley (HA 71) Close-up, Site Photographs, Well Hydrographs, and AOI EVI-PPT Graph for Northern Part of the Valley	62
Appendix 1-14. Edwards Creek Valley (HA 71) Close-up, Site Photographs, and AOI EVI-PPT Graph for West-Central Part of the Valley	64
APPENDIX 2 - Database Documentation	66
APPENDIX 3 – Summary Table of Results from Water Level, EVI, and PPT Trend Analyses and Field Investigations.....	71

INTRODUCTION

Throughout valley floors of Nevada and the larger Great Basin, groundwater dependent ecosystem (GDEs) represent hotspots of biodiversity, providing pockets of rich mesic habitat in an otherwise arid landscape. Despite their integral ecological role, little is known about long-term spatiotemporal responses of GDEs to changes in climate, hydrology, and land management. Surface and groundwater development for irrigation has stressed wetland, riparian, and phreatophyte shrubland communities in many areas. Identifying and documenting areas of stress both in space and time has been a challenge for numerous reasons, but primarily there is a lack of in-situ or remote observations. Utilizing the Landsat archive paired with spatially distributed reanalysis climate data and groundwater levels provides a unique opportunity to assess GDE long-term (i.e., >30 years) variability, trends, and potential drivers of change.

OBJECTIVES

The objectives of this project were to: 1) identify patterns of phreatophyte vegetation vigor change through space and time using the 30+ year Landsat archive and calculated vegetation index time series, and develop per-pixel trends and p-values based on Mann-Kendall non-parametric trend test and Sen's estimate of slope, and 2) qualitatively assess correlations between changes in phreatophyte vegetation vigor and precipitation, evaporative demand, and depth to groundwater (DTW) for selected Hydrographic Areas (HAs), and 3) summarize all results within a geographic information system (GIS) and numeric database of groundwater well locations, phreatophyte shrub areas, groundwater levels, and site photographs for selected HAs where shallow groundwater levels have declined over at least 10 years. The purpose of this data report is to briefly describe previous work, the approach and methods used in this study, numeric and GIS database structure and contents, and interpretation of selected results.

BACKGROUND & PREVIOUS WORK

Phreatophytes obtain their water requirement from surface water, groundwater, or both, through root systems that range from shallow to 18 m depth (Robinson, 1958; Glancy and Rush, 1968; Dawson and Pate, 1996). Phreatophytes can be classified into two categories, obligate or facultative, which relate to their levels of groundwater dependence. Obligate phreatophytes are groundwater dependent – they only inhabit areas where they can access groundwater. Facultative phreatophytes are not groundwater dependent – they inhabit areas where they can access groundwater, but also inhabit areas where their water requirements can be met by precipitation derived soil moisture reserves alone. Facultative phreatophyte species common in the Great Basin include greasewood (*Sarcobatus vermiculatus*), rabbitbrush (*Ericameria nauseous*), and basin big sagebrush (*Artemisia tridentata* spp. *tridentata*). While these facultative phreatophyte shrub species are known to consume groundwater, studies have concluded that they primarily rely on shallow soil water

derived from precipitation, and only consume harder to access groundwater during summer and early fall when shallow soil moisture levels are low (Albright et al., 2006; Chimner and Cooper, 2004; Dawson and Pate, 1996). However, a recent study in Dixie Valley, Nevada found that greasewood predominantly used groundwater throughout the entire year (Garcia et al., 2015).

Groundwater pumping for irrigation commonly results in lowering of the groundwater table (i.e., phreatic surface), leading to reduced phreatophyte groundwater evapotranspiration (ET_g) and vegetation vigor (Bredehoeft, 2002; Nichols, 2000, Elmore et al., 2003; Naumburg et al., 2005; Cooper et al., 2006; Patten et al., 2008; Groeneveld, 2008). Reduced ET_g due to groundwater pumping reflects the capture of natural groundwater discharge – the direct result of the law of conservation of mass. Since obligate phreatophyte species depend on groundwater, lowering of shallow groundwater levels would likely cause a transition to a different plant community (Stromberg et al. 1996). However, facultative phreatophyte species do not necessarily require groundwater and can survive on precipitation alone, so understanding and predicting vegetation response from lowering of the shallow groundwater is more uncertain and complex than for obligate species. This uncertainty has led to detailed reviews and studies on the effects of shallow groundwater declines on phreatophyte vegetation response.

Stromberg et al. (1996) found that depending upon the initial vegetation and depth to water table, a permanent water table decline could result in vegetation changing from obligate phreatophytes to facultative phreatophytes, and ultimately to non-phreatophytic upland species. Naumburg et al. (2005) reviewed past and current research at the time, and concluded that additional environmental and biological factors play important roles in vegetation response to shallow groundwater level decline. Naumburg et al. (2005) developed two conceptual models to highlight these additional factors and dependencies that include the rate of groundwater level decline, soil type, potential root growth rate, and maximum potential rooting depth. Additionally, climate is identified as an important factor, specifically precipitation timing and amount. Naumburg et al. (2005) suggest that the use of an ecological dynamics simulation model (EDYS) (Childress and McLendon, 1999; Childress, 1999; Childress et al., 1999) is needed to address and predict vegetation response to water table fluctuations, and whether these responses are gradual or threshold responses.

It is argued here that while models such as EDYS are important and perhaps needed to potentially identify gradual or threshold responses, an immediate first step is to simply identify where vegetation response has already occurred, and gather and organize the necessary information to relate vegetation responses to changes in the environment (e.g., DTW and annual precipitation). This study highlights data collection efforts focused on remotely sensed vegetation, measured groundwater levels, and modeled climate that will ultimately help better understand where vegetation change has already occurred and how these changes relate to changes in groundwater levels and climate. These basic datasets can

be used to provide needed information to support future prediction of phreatophyte vegetation response as a function of changes in groundwater levels, climate, and other factors.

APPROACH

In order to identify where phreatophyte vegetation responses have already occurred, an approach that paired remotely sensed satellite imagery with climate data and field investigations was developed. This approach was chosen due to the extremely large areas that phreatophyte shrubs occupy, along with the long time history required to adequately assess vegetation response (ideally 30+ years) with groundwater and climate variability. Recent advances in remote sensing and computational research using Landsat satellite imagery and gridded weather data for mapping vegetation vigor and estimating ET_g has provided an excellent opportunity for improving our understanding of historical and current phreatophyte conditions along with long term trends as they relate to local groundwater levels and climate. The Landsat satellite image archive is ideal for monitoring phreatophyte areas due to the continuity of the archive over the relatively long time period of 1984-present, and relatively high spatial resolution of 30 m x 30 m for optical bands. Landsat imagery has been freely available since 2009. Images acquired by the Landsat 5 Thematic Mapper (TM) are collected every 16 days; however, this interval is reduced to 8 days when combined with the Landsat 7 Enhanced Thematic Mapper Plus (ETM+) and Landsat 8 Optical Land Imager (OLI) satellites. Free access to the entire Landsat archive, combined with free access to the downscaled National Land Data Assimilation System (NLDAS; Mitchell et al., 2004) daily gridded climate data (gridMET; Abatzoglou, 2013) for estimation of water year precipitation and reference evapotranspiration (ET_o) (i.e., evaporative demand of the atmosphere), and cloud computing on the Google Earth Engine (GEE) (Gorelick et al., 2017) has provided a unique opportunity to assess GDE states and trends from 1985 to present. These states and trends can then be assessed with respect to climate and groundwater level changes.

The general approach implemented in this study was 1) identify a selected number of HAs (Table 1) where shallow (~0-30 ft below ground surface) groundwater levels have declined due to groundwater pumping, 2) perform Landsat based vegetation index trend analyses at the per-pixel level, and 3) use this information to guide and perform field investigations for selected HAs during the summer of 2017, 4) develop a site visit and photograph and GIS database, and 5) provide brief interpretations based on historical information, vegetation index and groundwater level trends, site visits, and respective climate variability for selected HAs. Originally, 12 HAs were identified for potential analysis, however, due to budget and project time constraints, six HAs were analyzed and summarized (Figure 1; Table 1). The theoretical basis and methods used in the approach are discussed below.

Table 1. Hydrographic Areas analyzed and visited for field investigation and database development.

Hydrographic Area Number	Hydrographic Area Name
30A	Kings River Valley
33A	Quinn River Valley
56	Upper Reese River Valley
69	Paradise Valley
71	Grass Valley
133	Edwards Creek Valley

METHODS

To address the objectives outlined above, numerous project datasets were developed and analyzed, including Landsat images, gridded climate data, groundwater levels, field photographs and documentation, and field site GIS data and photograph attribution.

Landsat Image Processing

Multiple Landsat image processing steps were performed using the GEE environmental monitoring platform. Landsat data processing for each study area was performed largely following methods outlined in Huntington et al. (2016) and Beamer et al. (2013). The Landsat TM, ETM+, and OLI top of atmosphere reflectance was transformed to at-surface reflectance following Landsat ecosystem disturbance adaptive processing system (LEDAPS) (for TM and ETM+) and Landsat Surface Reflectance Code (LaSRC) (for OLI) atmospheric correction algorithms (Schmidt et al., 2013; USGS, 2018). Landsat derived at-surface reflectance was used to compute *EVI* as

$$EVI = 2.5 \times (\rho_{NIR} - \rho_{Red}) / (\rho_{NIR} + (6 \times \rho_{Red}) - (7.5 \times \rho_{Blue}) + 1) \quad (\text{Eq. 1})$$

where ρ is the at-surface reflectance, *NIR* is near infrared waveband, *Red* is the red waveband, and *Blue* is blue waveband (Huete et al., 2002). *EVI* was chosen over other indices such as the normalized difference vegetation index (*NDVI*) to be consistent with the approach of Beamer et al. (2013) and workflow already developed for estimating *ET*, and the fact that Beamer et al. (2013) found that *EVI* had slightly better correlation to *ET* than *NDVI*.

The time period of June through August is generally the most representative period to characterize peak growing season health and vigor of phreatophyte vegetation in the Great Basin (Groeneveld et al., 2007; Allander et al., 2009; Garcia et al., 2015). However, vigorous non-phreatophytic annual grasses and forbs growing in phreatophyte shrub interspace during June through August can cause estimated phreatophyte *EVI* to be artificially inflated. Non-

phreatophytic annual grasses and forbs are commonly observed during the peak growing season, and noted to confound vegetation index – phreatophyte plant cover relationships (Garcia et al., 2015). To reduce the influence of annual grasses and forbs in estimating representative phreatophyte *EVI*, Landsat 5 images used in this study were limited to the period of July 15 to September 15. Additionally, this late summer period is optimal for assessing interannual variability in vegetation vigor due to shallow groundwater level variability since precipitation and soil moisture is typically at a minimum (Huntington et al., 2016). Image pixels were automatically flagged as clouds or shadows using the Fmask algorithm (Zhu and Woodcock, 2012) and were removed from the analysis. Other variables such as NDVI, normalized difference water index (NDWI), albedo, and surface temperature were used to assist in quality assurance and quality control (QAQC) of *EVI* time series.

Interannual *EVI* trends were computed using the Mann-Kendall trend test (Helsel and Hirsch, 1992). The Mann-Kendall trend test statistically assesses if there is a monotonic trend, upward or downward, in a variable over time. A monotonic trend means that the variable consistently increases or decreases in time, and the trend may or may not be linear. The Mann-Kendall test provides an advantage over the commonly used parametric linear regression analysis, since the Mann-Kendall test does not require that the residuals be normally distributed (i.e., the Mann-Kendall test is a non-parametric distribution-free test). The Mann-Kendall trend test was applied to 33 annual mean *EVI* images (i.e., one image for each year, from 1984-2017), where each *EVI* image is the mean July 15 to September 15 *EVI* for the year. The trend test returns the Sen's slope of annual *EVI* and respective p-values to assess the statistical significance of the annual *EVI* slope. The test was performed for every pixel in the image to ultimately make Sen's slope and p-value images. To address potential autocorrelation of annual *EVI* and PPT time series, two sample areas where *EVI* declined, and where *EVI* was stable, were assessed. Results indicated there was no statistically significant autocorrelation (assuming a one-year lag) for annual *EVI* or PPT for both areas analyzed. For future studies a more rigorous autocorrelation analysis could be applied, such as performing a per-pixel Durbin-Watson test. Another approach would be to use autoregressive integrated moving average (ARIMA) models (Box and Jenkins, 1970) for long enough time series (at least 20-30 years) to test for all lags and estimate confidence intervals to increase the chance of detecting longer lags such as El Niño cycles.

Groundwater Level Database

Groundwater level data was obtained from the Nevada Division of Water Resources (NDWR) water level database (<http://water.nv.gov/WaterLevelData.aspx>). Two water level readings per year were typically reported, once in spring before the irrigation season and one in fall after the irrigation season, therefore an average of the two readings was computed for each year. Water level measurements reported for 2017 are only based on one measurement recorded in March due to the time at which the database was downloaded from NDWR and processing for this study began. In addition to including the standard site information (e.g.,

well depth, well log, well name, perforation interval, basin, owner, etc.), the annual water level database was processed and summarized per well with the following variables: measurement start date, measurement end date, number of observations, water level minimum, maximum, mean, and median over the period of record, and the Mann-Kendall trend test derived Sen's slope of annual water level rise or decline. This summary database was joined to the GIS site database, so that well locations could be attributed with water level trends and displayed on a map in combination with *EVI* trends.

Site Visits, GIS, and Photograph Database

Site visits conducted during the summer of 2017 were determined by visualizing groundwater level trends along with *EVI* trends in ArcGIS to identify areas within the groundwater discharge area where both *EVI* and groundwater levels were declining. Land ownership, road access, and travel distances were all considerations in selecting the field sites, so sites were typically limited to 3 to 10 per HA. Once at the site, field investigators would take multiple site photographs and would record the location, location FID (i.e., feature ID for each photograph location), date, photograph ID, DTW based on nearby well information, plant and/or community type, and if any impacts were visible such as qualitative indicators of stress (e.g., reduced vigor, canopy loss, or discoloration) or mortality. Records were then input into a GIS database and site photographs were linked to each site by creating cloud storage photograph hyperlink URLs, and including URLs within the GIS attribute table for each site. Lastly, representative areas of interest (AOIs) were digitized in GIS around select field sites, to spatially average annual *EVI*, precipitation (*PPT*), and reference evapotranspiration (*ET_o*) and assess respective time series, correlations, and trends at select sites. *ET* and *ET_g* was also computed for each AOI following the approach of Beamer et al. (2013) and included in the database package. A FID (i.e. feature ID) within the GIS database, figures, and appendices of this report uniquely identifies photograph locations and AOIs for each basin. FIDs for the photograph location features and AOI features begin at 0 and increase numerically by 1.

Gridded Climate Data Processing

Annual *PPT* and reference *ET_o* for each AOI was estimated using 4 km spatial resolution North American Land Data Assimilation System (NLDAS; Mitchell et al., 2004) and Parameter Regression on Independent Slopes model (PRISM; Daly et al., 2008) hybrid meteorological data (gridMET; Abatzoglou, 2013), in which a representative 4 km cell was chosen for each AOI. Annual *ET_o* for each phreatophyte area was estimated from water years 1984 to 2017 for each site using gridMET daily values of solar radiation (*R_s*), maximum temperature (*T_{max}*), minimum temperature (*T_{min}*), average dew point temperature (*T_{dew}*), and wind speed at 10 m height (*u₁₀*). Meteorological variables were used to compute *ET_o* with the ASCE-EWRI Standardized Penman-Monteith (ASCE-PM) reference ET equation (ASCE-EWRI, 2005) for a short grass reference. The ASCE-PM equation requires 2 m height

equivalent wind speed, therefore 10 m height wind speed was logarithmically transformed to 2 m height equivalent following ASCE-EWRI (2005).

RESULTS

For each HA investigated, field site descriptions and trends in EVI and groundwater levels are summarized, and historical information is highlighted based on reconnaissance series reports and water resource bulletins conducted in the early 1960s. Select site photographs and well hydrographs are referenced in the discussion of results, and can be viewed in Appendix 1. Entire collections of site photographs and well hydrographs for each basin, as well as GIS files and trend maps can be found within the database prepared for this report. A full description of the database is given in Appendix 2. A table summarizing water level trends for each well, trends in EVI at field sites, trends in PPT for AOIs, and vegetation status at field sites is given in Appendix 3.

Kings River Valley (HA 30A)

Trends in EVI and DTW at each well along with field-investigation photograph locations and phreatophyte boundaries are shown in Figures 2 and 3. Phreatophyte shrubland communities are primarily composed of greasewood, sagebrush, and desert thorn. Sagebrush and desert thorn showed signs of stress along the moderate to densely vegetated eastern parts of the valley (Appendix 1-1; photograph locations (FIDs 2-4); photographs (pc_number 526-528)), however, greasewood did not show signs of stress in the shrub communities. DTW in this area has increased from roughly 40 to 90 ft (1998-2016) (Appendix 1-1; hydrographs for wells 030A N45 E34 29ABBC1; 030A N45 E34 29ABBC2). A greasewood monoculture of moderate density in the north-central part of the valley (near irrigated area) showed signs of stress and was less vigorous than the greasewood along the eastern part of the valley. The DTW at the irrigated area just west of the region has increased from 50 ft to more than one 100 ft (1995-2016). Greasewood and sagebrush communities dominate shrublands in the southeast part of the valley; sagebrush showed signs of stress and some mortality, whereas greasewood seemed to be thriving (Appendix 1-2; photograph location (FID 11); photograph (pc_number 541)). Sagebrush monocultures in the southeast part of the HA also showed signs of stress (Appendix 1-2; photograph location (FID 12); photograph (pc_number 542)). Depths to groundwater measured at the irrigated areas just north of this region have increased from 50 ft to 80 ft (1994-2016) (Appendix 1-2; hydrograph for well 030A N44 E34 16AAA1). EVI and groundwater level trends generally support these findings at field site locations (Figure 2); however, many of the trends are not statistically significant at the 90% confidence level within the phreatophyte boundary (Figure 3). Interannual EVI largely covaries with water year PPT from within AOIs 1984-2017 (Appendix 1-1 and 1-2; FIDs 0-3), and no obvious deviations from multi-year PPT variability is apparent.

Groundwater pumping for irrigation within the valley started well before the beginning of the spectrally consistent Landsat 5, 7, 8 archive (i.e. 1984). According to Zones (1963), groundwater pumping for irrigation began in 1956, and DTW within the phreatophyte boundary at that time ranged from <10 to 40 ft. According to the NDWR water level database, minimum DTW within the phreatophyte boundary ranges from 6 ft to 213 ft,

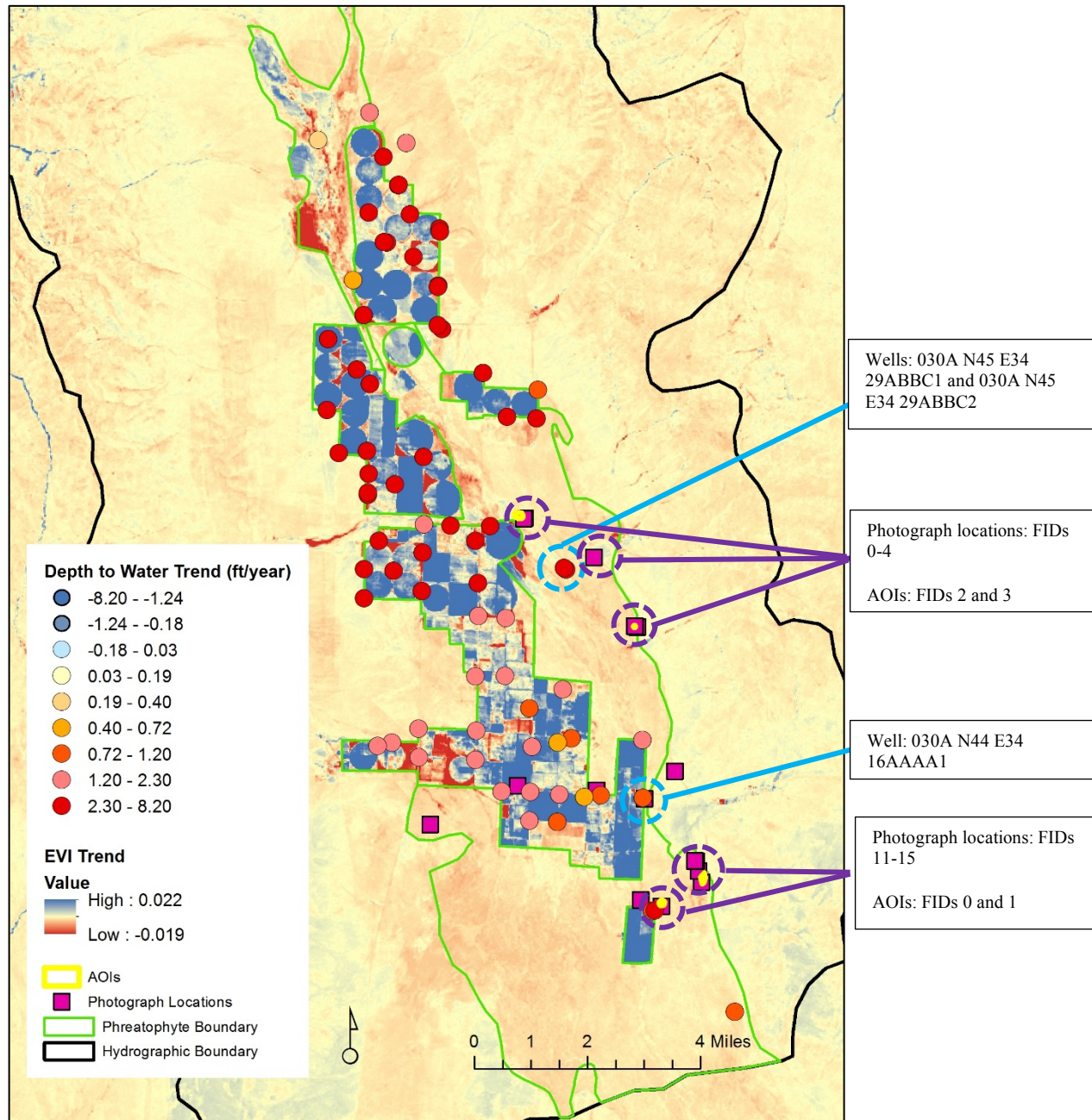


Figure 2. Kings River Valley (HA 30A) groundwater level and EVI trends, site photograph locations, and AOIs.

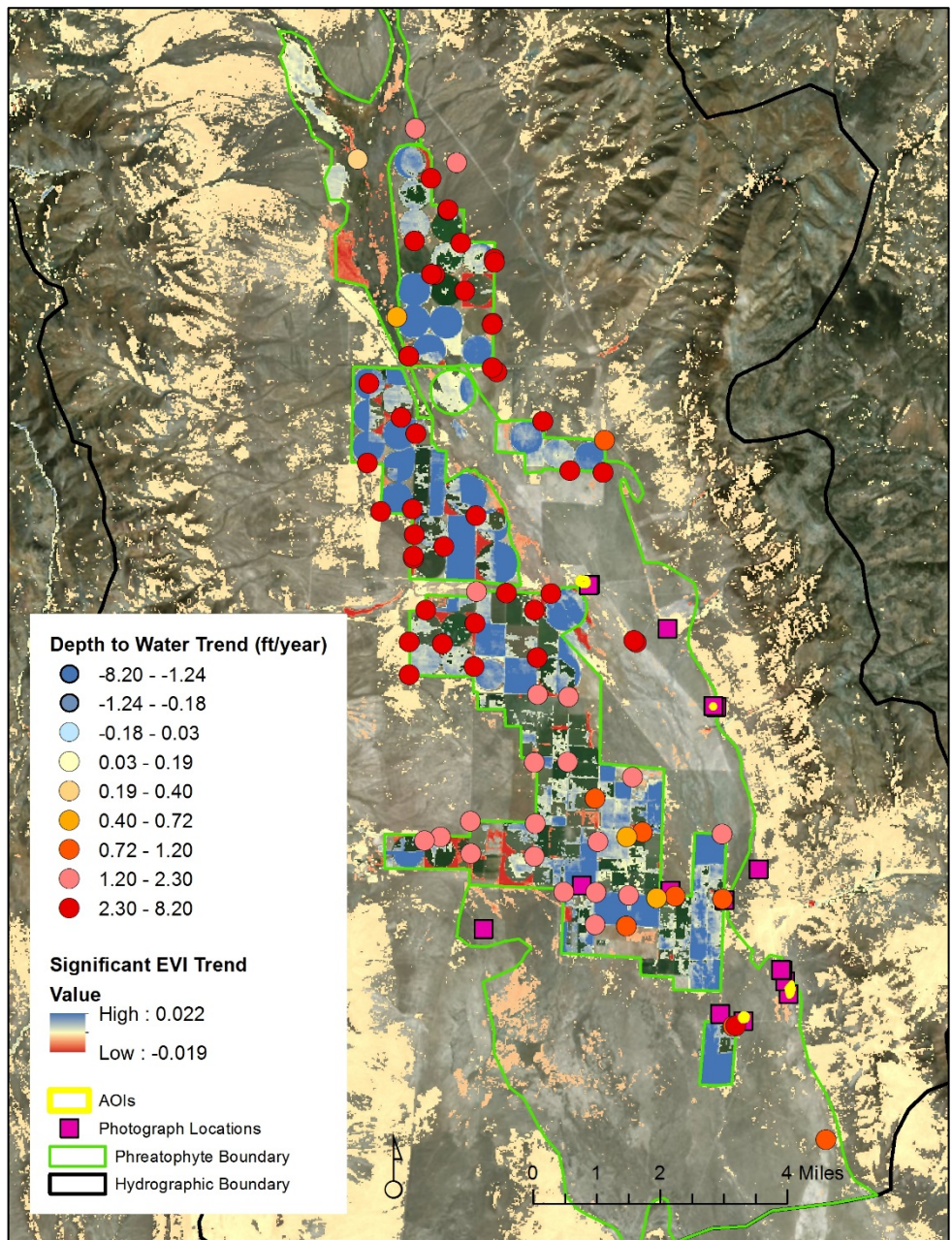


Figure 3. Kings River Valley (HA 30A) groundwater level and EVI trends, and site photograph locations, and AOIs. EVI trend pixels were masked out if p-values were greater than 0.10.

with an average 84 ft from 1989 to 2016. The earliest NDWR database measurement date is 1989 (about half of the wells), and for those wells in 1989, the minimum DTW within the phreatophyte boundary ranged from 36 to 156 ft, with an average 77 ft. According to Zones (1963):

“Greasewood is the most common phreatophyte in Kings River Valley; others are saltgrass, ryegrass, rabbitbrush, meadow grasses, willows, and associated wild rose, buckbrush, and pickleweed. In addition, about 1,000 acres of meadow grasses and alfalfa are supported in part by flood irrigation and in part by roots that tap the ground-water reservoir. Phreatophytes are thickest along the axis of the valley, particularly at the north end. A few small isolated areas of densely growing phreatophytes also occur at the base of the mountains. The phreatophytes in the valley usually are limited to areas where the depth to water is less than 25 feet.”

“Ground-water withdrawals increased markedly in 1958, when about 17,000 acre-feet was pumped from 23 wells, all of which are in the northern part of the valley. The water was used to irrigate about 5,000 acres of wheat and other grains, potatoes, and alfalfa. The effects of the recent heavy pumping on the ground-water levels are noted in figures 2 to 4. Figure 2, based largely on water levels reported by drillers, show the piezometric surface before heavy pumping began; figure 3 shows the piezometric surface in January 1959; and figure 4 shows it in October 1959. The maps indicate that general declines of water level in the areas of heaviest pumping – 10 to 30 feet in the southeastern part of T.46 N., R. 33 E., and about 10 feet in the eastern part of T. 45 N., R. 33 E. The maps indicate also that groundwater is being diverted from the areas of natural discharge – that is, from the phreatophyte areas toward the pumped areas.”

Malmberg and Worts (1966) conducted a study in Kings River Valley focused on evaluating the effects of pumping on the general hydrology of the basin. Malmberg and Worts (1966) developed a groundwater level net-change map for the period of 1957-1964 (shown in Figure 4) and made the following statements:

“The maximum declines in and near the centers of pumping are 30 to 40 feet. The smallest net declines in the area of pumping, not much more than 10 feet, occurred beneath the Kings River Channel, which during times of

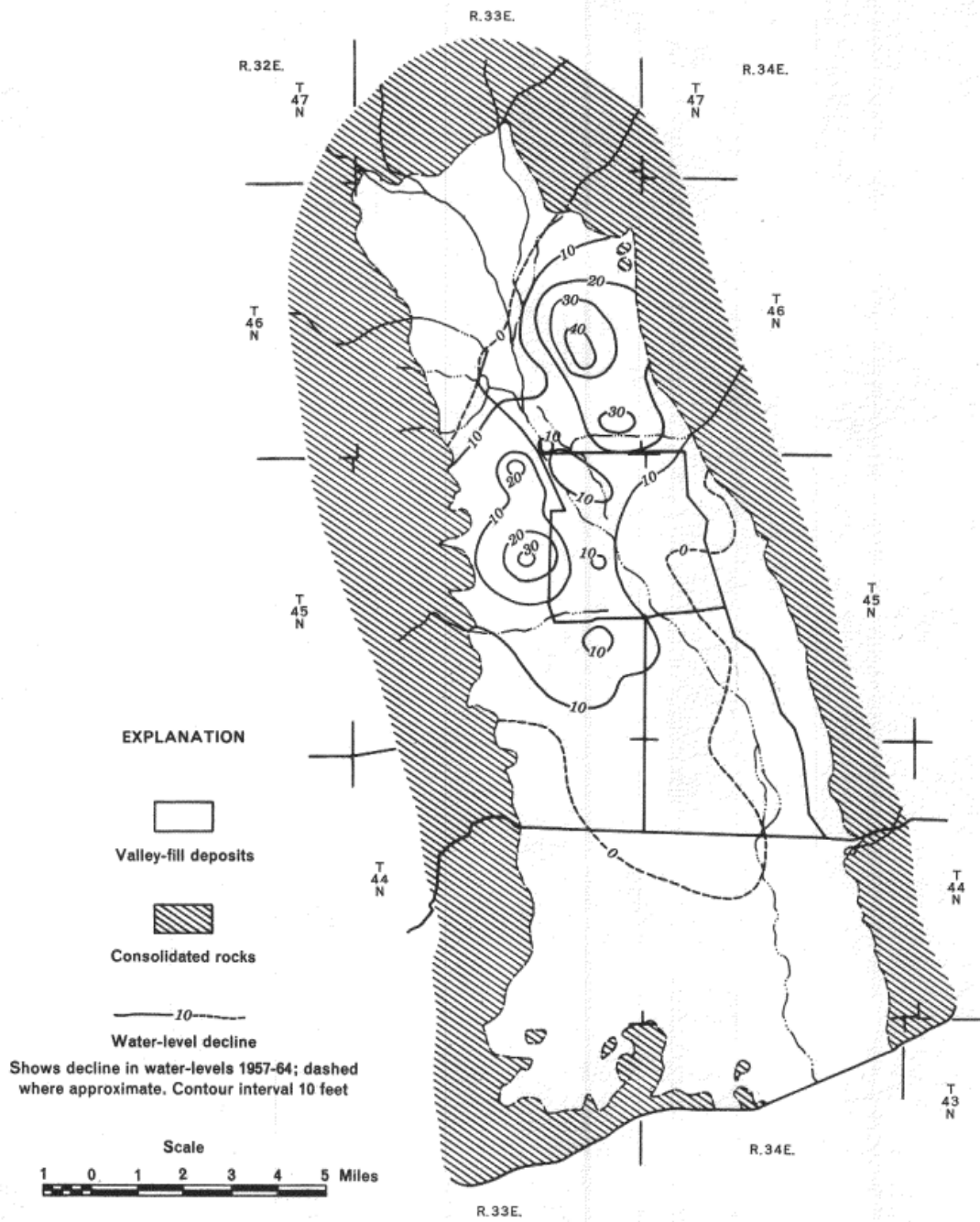


Figure 4. Distribution of DTW changes within Kings River Valley as reported by Malmberg and Worts (1966).

flow, forms a line source of recharge, or a recharge boundary. The weighted average areal net decline for the Rio King subarea was between 10 and 11 feet.”

“In the period 1957-63, nearly 4,000 acres of phreatophytes were eliminated by land clearance and replaced by irrigated crops. In addition, the water level beneath roughly 20,000 acres of phreatophytes declined an average of about 10 feet. Assuming nearly 1000 percent transfer of natural evapotranspiration losses to consumptive use by crops in the irrigated areas and assuming a 20 percent reduction of evapotranspiration losses in the remaining area of water-level decline, the salvage in 1963 amounted to between 1,200 and 1,500 acre-feet. Thus, evapotranspiration losses in 1963 probably were about 8,000 acre-feet compared to 9,400 acre-feet under natural conditions from the same area.”

“If all the permitted rights to pump about 60,000 acre-feet per year were exercised by 1973 (10 years hence) and if the increase in pumping between 1963 and 1973 were reasonably uniform, storage depletion (1957-73) could be on the order of 250,000 acre-feet. This estimate is based on several major factors: (1) evapotranspiration losses would continue to decrease and would become negligible by 1973; (2) groundwater and surface-water outflow would decrease to about one-half their present average amount; (3) surface water diversions would be decreased to about half the 1963 rate...” “In terms of water-level declines, a storage depletion on the order of 250,000 acre-feet is equivalent to a subarea-wide decline of nearly 20 feet, based on the estimate in table 9. However, in the centers of pumping, the actual declines probably would be more than 100 feet below the March 1964 levels and less than 20 feet in those parts of the subarea remote from pumping.”

Given these factors and historical context, a substantial portion of the vegetation change has likely already occurred, and significant vegetation changes within the Landsat archive (1984-2017) has likely been minimal relative to those that occurred a few decades after the onset and continuation of pumping since the late 1950s and early 1960s. The average pumpage from 2011 to 2015 in Kings River Valley is reported by NDWR to be approximately 50,000 acre-feet per year over 13,000 irrigated acres (<http://water.nv.gov/Crop%20Inventories/2015/Kings%20River%20Valley.pdf>). Based on the NDWR water level database, groundwater levels are indeed currently more than 100 ft below 1964 levels within pumping centers, and have also declined more than 20 ft in areas away from the pumping and within the phreatophytes boundary as Malmberg and Worts (1966) suggested would occur. A noteworthy finding is that while some localized stress and

some mortality was reported from field investigations performed in this study, phreatophyte communities still persist within the discharge area even though DTW is now well below typically reported rooting depths in most areas (i.e. > 20 to 60 ft).

Quinn River Valley (HA 33A – Orovada Subarea)

Trends in EVI and DTW at each well along with field-investigation photograph locations and phreatophyte boundaries are shown in Figures 5 and 6. Phreatophyte shrubland communities are composed of greasewood, sagebrush, and rabbitbrush (*Ericameria nauseosa*). Densely vegetated phreatophyte communities in the north-central part of the HA generally show little signs of stress (Appendix 1-3; photograph location (FID 0); photograph (pc_number 521)). Rabbitbrush shows some signs of stress at the north-central part of the valley adjacent to riparian/meadow areas, however, greasewood in this area does not appear to be stressed (Appendix 1-3; photograph location (FID 0); photograph (pc_number 521)). The DTW in this area has varied from five to 20 ft since 2012 (Appendix 1-3; hydrographs for wells 033A N44 E36 26ACB1, 033A N44 E36 22DCAA1, 033A N44 E36 34ADBC1). Wells near the photograph location (identified above) reported a decrease in DTW of approximately 15 to 5 ft from summer 2016 to spring of 2017 likely due to the above average 2017 water year (150% of normal). At the northwest part of the valley near a spring (western most photograph points shown in Figure 5), sagebrush within a sparsely vegetated community of greasewood shows signs of stress and mortality (Appendix 1-4; photograph locations (FIDs 1 and 2); photographs (pc_number 522 and 523)). DTW in this area has been highly variable, both increasing and decreasing with water year PPT. DTW increased from approximately 3.5 to 7 ft near the spring discharge area since 2007 (Appendix 1-4; hydrographs for wells 033A N44 E36 33BCDA1; 033A N43 E36 04DDDD1). EVI and groundwater level trends generally support these findings (Figures 5 and 6). The majority of the EVI trends are not statistically significant at the 90% confidence level within the phreatophyte boundary (Figure 6), however, there is a large contiguous area of significant EVI decline located within the corridor of the Quinn River, and western margin of the phreatophyte boundary (i.e., near the western most photograph points near the spring discharge area). DTW for wells within or directly adjacent to the Quinn River indicate that DTW has increased from 8 to 22 ft over the last 10 to 24 years (Appendix 1-5; hydrographs for wells 033A N43 E36 14BCBB1; 033A N42 E36 08AAB1; 033A N41 E36 06ABBB1; 033A N41 E36 06CBAA1) - identified from north to south along the riparian area), and supports statistically significant EVI declines within the riparian area. Similar to what is illustrated from the hydrograph within the spring discharge AOI located around the western most photograph location (i.e., hydrograph for well 033A N44 E36 33BCDA1), interannual EVI largely covaries with water year PPT within the AOI (Appendix 1-4; AOI FID 0), and no obvious deviations from multi-year PPT variability is evident. Similar to Kings River Valley, groundwater pumping for irrigation within the valley started well before the

beginning of the spectrally consistent Landsat 5, 7, 8 archive (i.e., 1984). According to Huxel (1966), groundwater pumping for irrigation began in the late 1940s and was accelerated by the disposition of public land under the Desert Land Entry Acts. DTW within the phreatophyte boundary as of 1963 ranged from <10 to 30 ft.

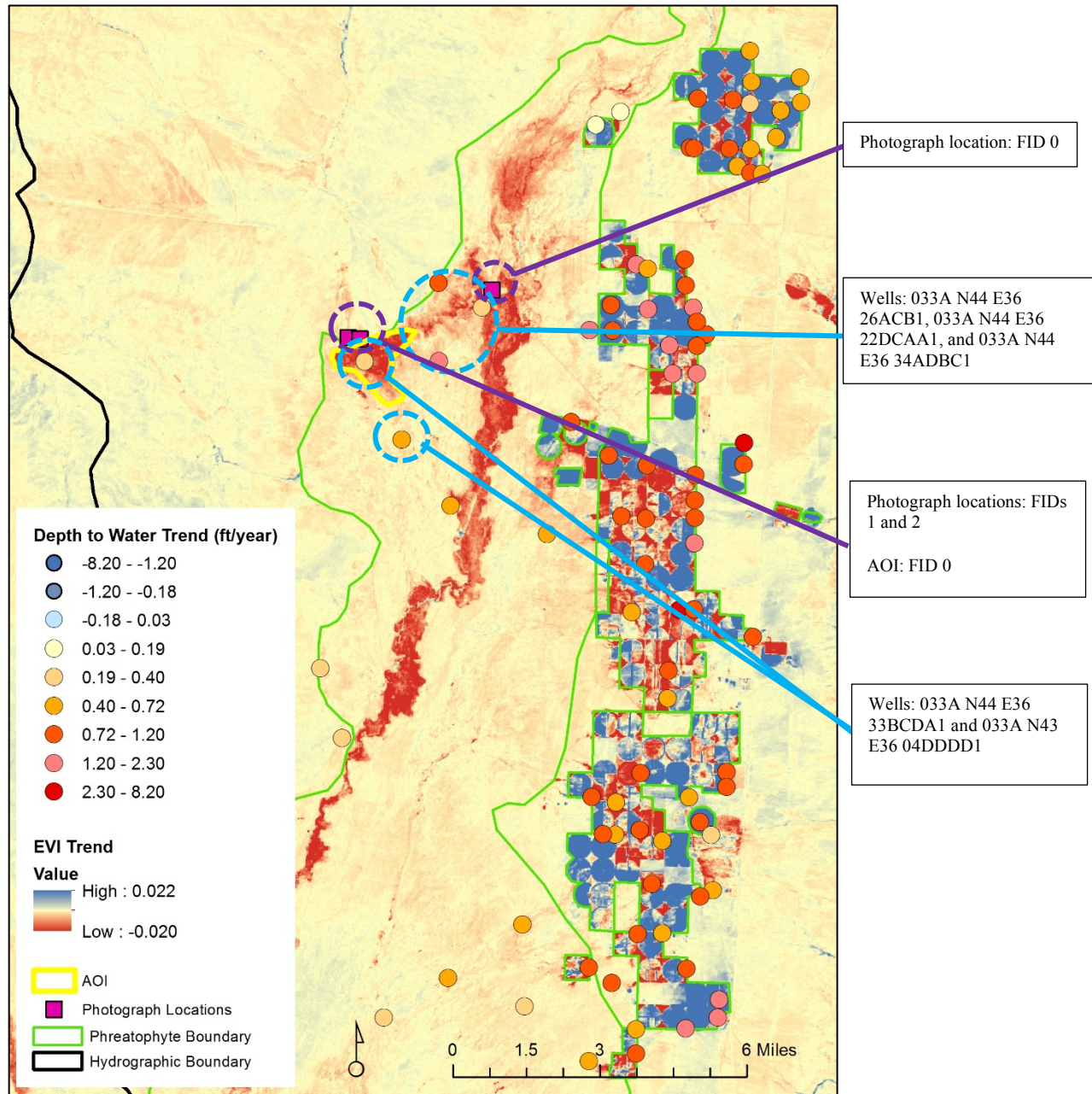


Figure 5. Quinn River Valley (HA 33A) groundwater level and EVI trends, site photograph locations, and an AOI.

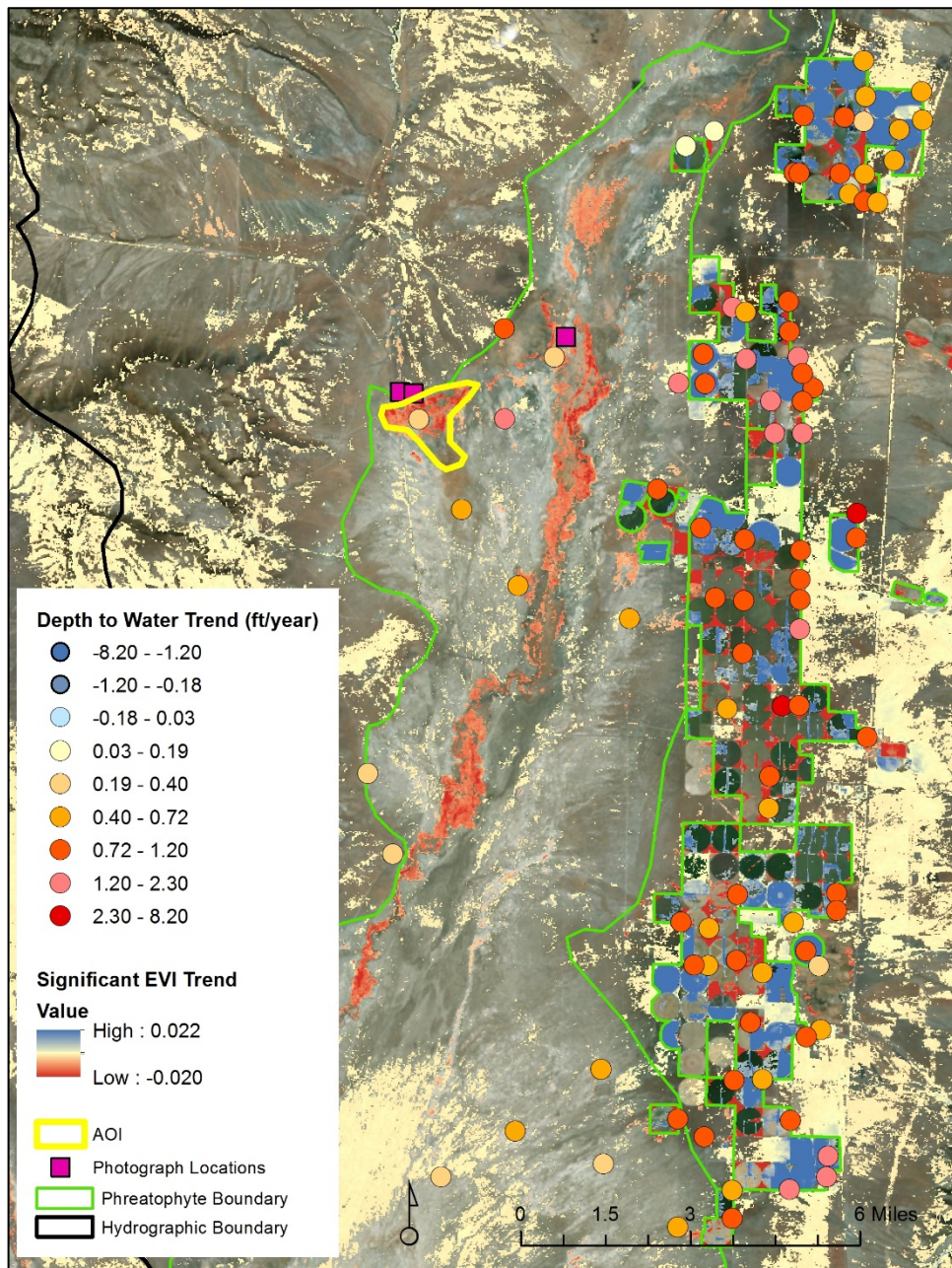


Figure 6. Quinn River Valley (HA 33A) groundwater level and EVI trends, site photograph locations, and an AOI. EVI trend pixels were masked out if p-values were greater than 0.10.

According to the NDWR water level database, minimum DTW within the phreatophyte boundary ranges from 3 to 55 ft, with an average 15 ft from 1991 to 2017. The earliest database measurement year varies from 1991 to 2014, where 3 to 4 measurement sites were added each year from 1991. According to Huxel (1966):

“The dominant phreatophytes are greasewood, rabbitbrush, saltgrass, rye grass, and native meadowgrass. Also present are minor assemblages of pickleweed, sumpweed, and buffalo berry.”

“By about 1955 about 20 irrigation wells were producing about 5,000 acre-feet of ground water annually. By 1964 nearly 115 irrigation wells had been drilled; 82 wells were pumped and discharged about 40,000 acre-feet. Additional wells are expected to go into production in the next several years.”

“The maximum net decline from the near equilibrium water levels in 1947 to the spring high water levels in 1964 is somewhat more than 25 feet. The weighted average areal net decline within the zero contour was about 12 feet, the area is about 75,000 acres.”

“The extent and magnitude of the future pumping effects are difficult to predict. Nevertheless, figure 9 shows that pumping effects have already reached the southernmost part of the McDermitt subarea, and over the long term probably would extend into the Silver State subarea. Although the amount of additional natural discharge that would be salvaged is also difficult to predict, probably most of the evapotranspiration loss in the Silver State subarea and possibly a fourth of the loss in the McDermitt subarea would eventually be salvaged. Thus, the preliminary estimate of the total discharge that may be salvaged is on the order of 50,000 acre-feet per year. This in turn suggests that by concentrating all the pumping in the Orovalada subarea, only about two-thirds of the potential yield of the Quinn River valley area will be realized.”

NDWR reports the 2011-2015 average irrigated acreage and pumping to be 18,000 acres and 63,000 acre-feet, respectively ([http://water.nv.gov/Crop%20Inventories/2015/Quinn%20River%20\(Orovalada%20Subarea\).pdf](http://water.nv.gov/Crop%20Inventories/2015/Quinn%20River%20(Orovalada%20Subarea).pdf)). Given that there has been substantial pumping since the early 1960s, the majority of vegetation change likely already occurred prior to 1984, so relative vegetation changes within the spectrally consistent Landsat archive (1984-2017) are probably minimal. However, EVI trends clearly show vegetation declines near shallow groundwater spring and riparian areas, and these areas were identified to have some localized stress and mortality as determined from field investigations performed in this study. Field investigations also show

that phreatophyte communities persist within the larger discharge area even though DTW is well below typically reported rooting depths in many areas (~20 to 60 ft).

Upper Reese River Valley (HA 56)

Trends in EVI and DTW at each well along with field-investigation photograph locations and phreatophyte boundaries are shown in Figures 7 and 8. Phreatophyte shrubland communities in the south-central part of the HA are primarily composed of greasewood, rabbitbrush, and sagebrush. Sparsely vegetated communities of sagebrush and rabbitbrush dominate at the southern edge of the groundwater discharge boundary. In this area sagebrush mortality is locally extensive, and rabbitbrush appears to be stressed (Appendix 1-6; photograph location (FID 0); photographs (pc_number 430-451)). A more densely vegetated community of rabbitbrush and sagebrush at the southeast side of the discharge boundary shows less signs of stress (Appendix 1-6; photograph location (FID 1); photographs (pc_number 452-462)). DTW in this area is unknown due to the absence of wells in the area. Northward along the southeastern side of the groundwater discharge boundary, communities of greasewood, rabbitbrush, and sagebrush show less signs of stress than the communities in the south (Appendix 1-7; photograph location (FID 3); photographs (pc_number 473-476)). A monoculture of moderately dense rabbitbrush in the southwestern part of the discharge area shows signs of stress (Appendix 1-8; photograph location (FID 6); photographs (pc_number 496-510)). However, a moderately dense community of greasewood and rabbitbrush north of this rabbitbrush monoculture does not show any signs of stress (Appendix 1-8; photograph location (FID 5); photographs (pc_number 484-495)), and two wells within this area indicate that DTW was larger at the northern site (roughly 20 ft) (Appendix 1-8; hydrographs for wells 056 N17 E42 06BBCC1; 056 N18 E42 19CABB1). DTW within the irrigated areas directly west of the groundwater discharge boundary has increased significantly since the 1960's, ranging from 20 to 40 ft. According to the NDWR water level database, for wells that began being measured between 1959 to 1968, DTW has increased by about 30 ft as of spring of 2017 (e.g. Appendix 1-8; hydrographs for wells 056 N17 E41 12DCCC1; 056 N17 E42 06BBCC1; 056 N17 E41 01BCBC1; 056 N18 E42 19CABB1). While no DTW information is available within the down gradient phreatophyte area, DTW has likely increased within the phreatophyte area. This hypothesized increase in DTW within the phreatophyte area is supported by declining EVI shown in Figure 7 and 8, and also supported from field investigations showing signs of localized stress.

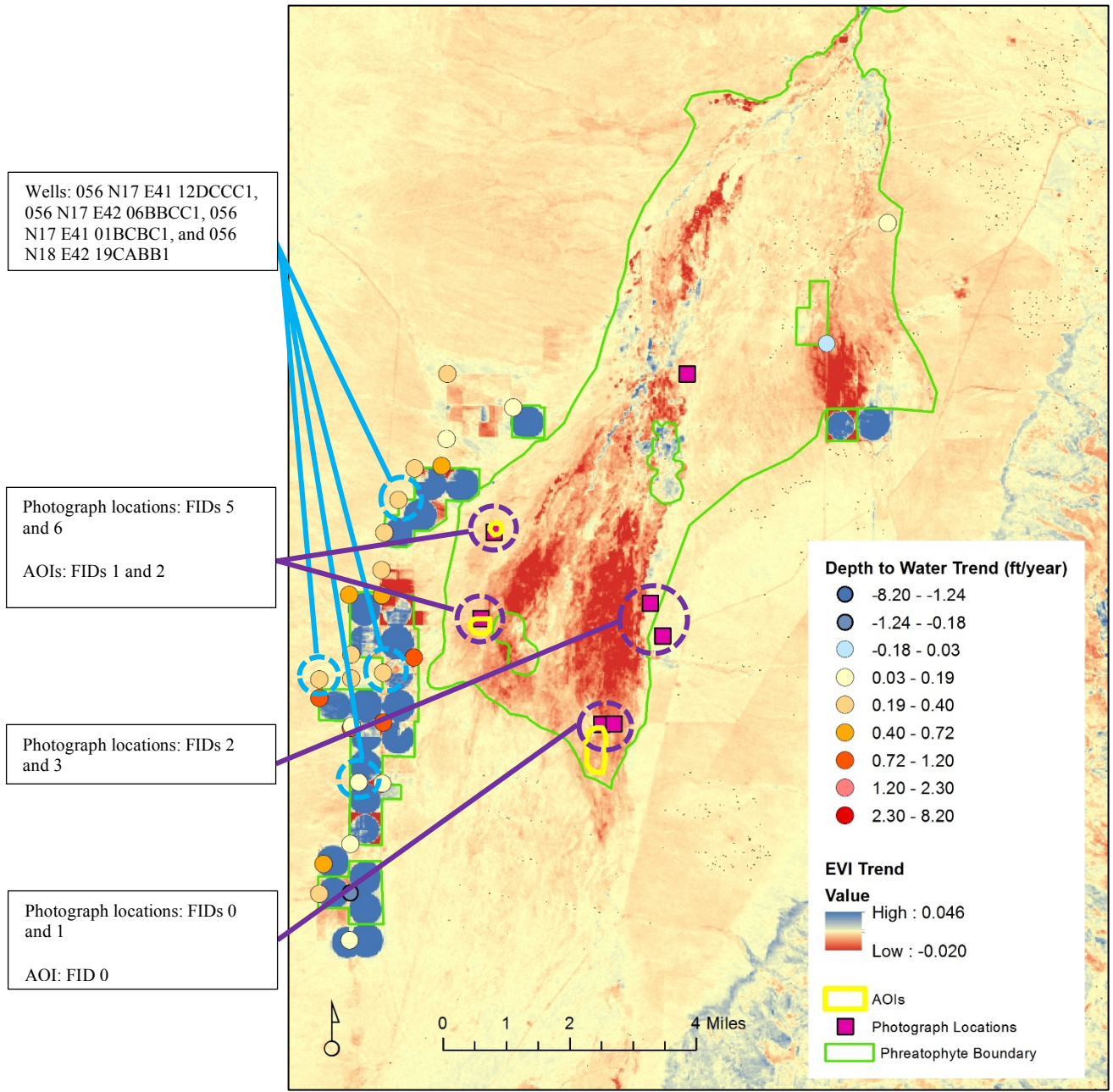


Figure 7. Upper Reese River Valley (HA 56) groundwater level and EVI trends, site photograph locations, and AOIs.

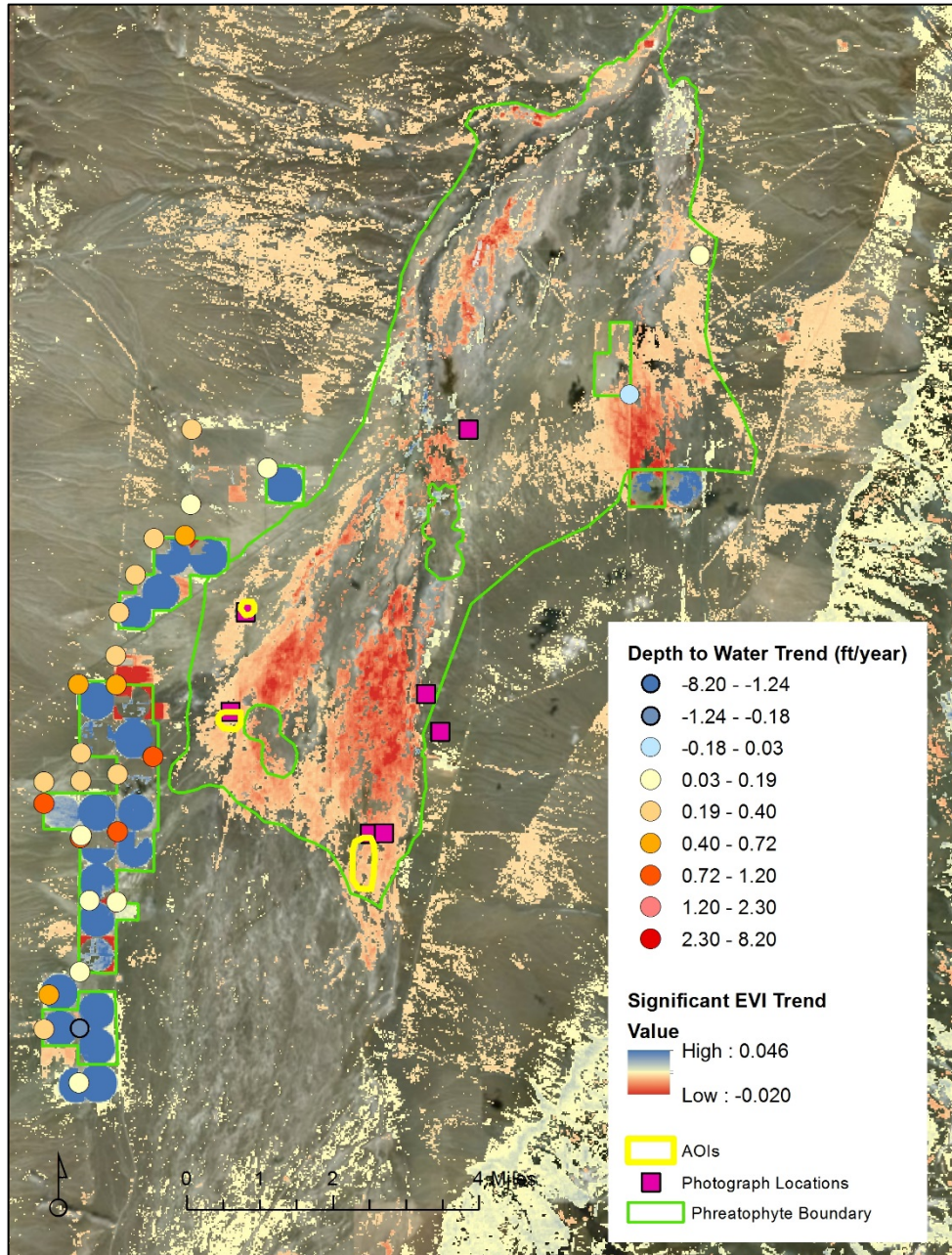


Figure 8. Upper Reese River Valley (HA 56) groundwater level and EVI trends, site photograph locations, and AOIs. EVI trend pixels were masked out if p-values were greater than 0.10.

The Upper Reese Valley reconnaissance series report of Eakin and Everett (1965) states:

“The present area of irrigation wells is on the west side of the main area of natural discharge of ground water in the upper Reese River Valley. Recharge from precipitation in the Shoshone range to the west and southwest of pumping is considered to be very minor. Pumping in this area therefore initially will be almost entirely from ground water in storage. Under continued pumping, water levels will be lowered at increasing distance from the well field until inflow equaled the rate of pumping. In this area, drawdown east of the well field will gradually extend into the adjacent area of natural discharge. The extent to which ground water is salvaged by this well field can be indicated by the extent to which ground water is diverted from the phreatophyte area to the wells. Continued pumping at the rate and seasonal pattern as used in 1964 probably will require several years before measurable drawdown will occur in the unconfined shallow ground water in the natural discharge area. Probably an additional several years pumping will be required before the drawdown and area included are sufficient to significantly reduce natural groundwater discharge in these areas. How soon, or whether pumping in this area would affect the discharge of the principal springs on the Gondolfo Ranch cannot be indicated with any assurance at this time. Until variations due to the natural conditions can be demonstrated, it would be difficult to compute any effect due to pumping in the new well field.”

Indeed, capture of natural discharge down gradient (east) of the irrigated area has likely occurred due to the fact that groundwater pumping began in the mid 1960s, and has increased since then. Google Earth Engine Landsat time lapse (<https://goo.gl/9fkjCz>) suggests that pumping has increased from 1984 to 2016 (due to increase in irrigated acreage that is clearly visible), and wheel line and flood irrigation has been converted to center pivot irrigation, leading to greater consumptive use, and less return flow. EVI trends shown in Figures 7 and 8 along with field investigation photographs support associated effects of groundwater capture within the down gradient phreatophyte areas (i.e., reduced vegetation vigor). Gandolfo Ranch is located near southeastern photograph locations shown on Figures 8, where significant negative EVI trends are evident, and field visit photographs and notes also indicate localized phreatophyte stress. Another large area of significant EVI decline is to the northeast, also an area down gradient of a spring. From inspection of Landsat time lapse on Google Earth Engine (<https://goo.gl/LjLUMT>), spring water was historically used for flood irrigating pasture grass, and groundwater pumping and center pivot irrigation directly south of the spring began in 2001. Since 2001, it appears that flood irrigation has declined, likely due to the capture of spring flow from groundwater pumping.

The AOI associated with southernmost photograph locations shown in Figures 7 and 8 indicate that while interannual EVI tracks closely with water year PPT, since about 2012 EVI has remained low even though water year PPT has been at or above normal, and EVI also shows a general downward trend (Appendix 1-8; AOI FID 0). Other AOIs associated with photograph locations on the western edge of the phreatophyte do not illustrate departure from water year PPT (Appendix 1-8; AOI FIDs 1 and 2). While EVI is generally trending downward within these AOIs, so is water year PPT.

Paradise Valley (HA 69)

Trends in EVI and DTW at each well along with field-investigation photograph locations and phreatophyte boundaries are shown in Figures 9 and 10. Phreatophyte shrubland communities south of the meadow/riparian areas are composed of greasewood, sagebrush, shadscale and rabbitbrush. A moderately dense community of greasewood, sagebrush and shadscale on the southeastern side of the groundwater discharge boundary shows little stress (Appendix 1-9; photograph location (FID 0); photographs (pc_number 358-362)). The DTW at two wells surrounding this area has increased by roughly 10 ft since 1991 (Appendix 1-9; hydrographs for wells 069 N38 E39 22ABAA1; 069 N39 E39 36CDCD1). A small community of sagebrush and rabbitbrush within the historical Gumboot Lake (east of Winnemucca Farms) shows signs of localized stress and mortality (Appendix 1-9; photograph location (FID 1); photographs (pc_number 363-367)). Depths to groundwater in this area have increased from 30 to 45 ft since 1991 (Appendix 1-9; hydrographs for wells 069 N38 E39 21AAA1; 069 N38 E39 28BAAA1). The southern part of the groundwater discharge area in Paradise Valley is composed of moderately dense communities of greasewood, sagebrush and shadscale; sagebrush and shadscale show some signs of stress, whereas greasewood appears to be unaffected (Appendix 1-10; photograph location (FID 8); photographs (pc_number 410-419)). The DTW at this site has increased from roughly 20 to 35 ft since 1991 (Appendix 1-10; hydrograph for well 069 N37 E38 24ACC1). The meadow/riparian areas of the northern part of Paradise Valley showed little signs of stress (Appendix 1-11; photograph locations (FIDs 2 and 3); photographs (pc_number 368-372)), even though EVI trends indicate significant declines (Figures 10). Russian olive and buffalo berry tree species were the only vegetation that appeared to be stressed within the meadow/riparian area (Appendix 1-11; photograph location (FID 4); photographs (pc_number 381-386)). The DTW in this area has increased by roughly 5 to 10 ft since 1994 (Appendix 1-11; hydrograph for well 069 N39 E39 04BDC 1; 069 N40 E39 22CBAB1; 069 N40 E39 24CBDA1). Shrublands along the western side of the groundwater discharge boundary (adjacent to meadow/riparian areas in the north) are composed of greasewood and sagebrush; sagebrush shows signs of localized stress, whereas greasewood appears to be unaffected (Appendix 1-11; photograph locations (FIDs 5-7); photographs (pc_number 387-396 and 403-409)). Depths to groundwater in along the western part of the

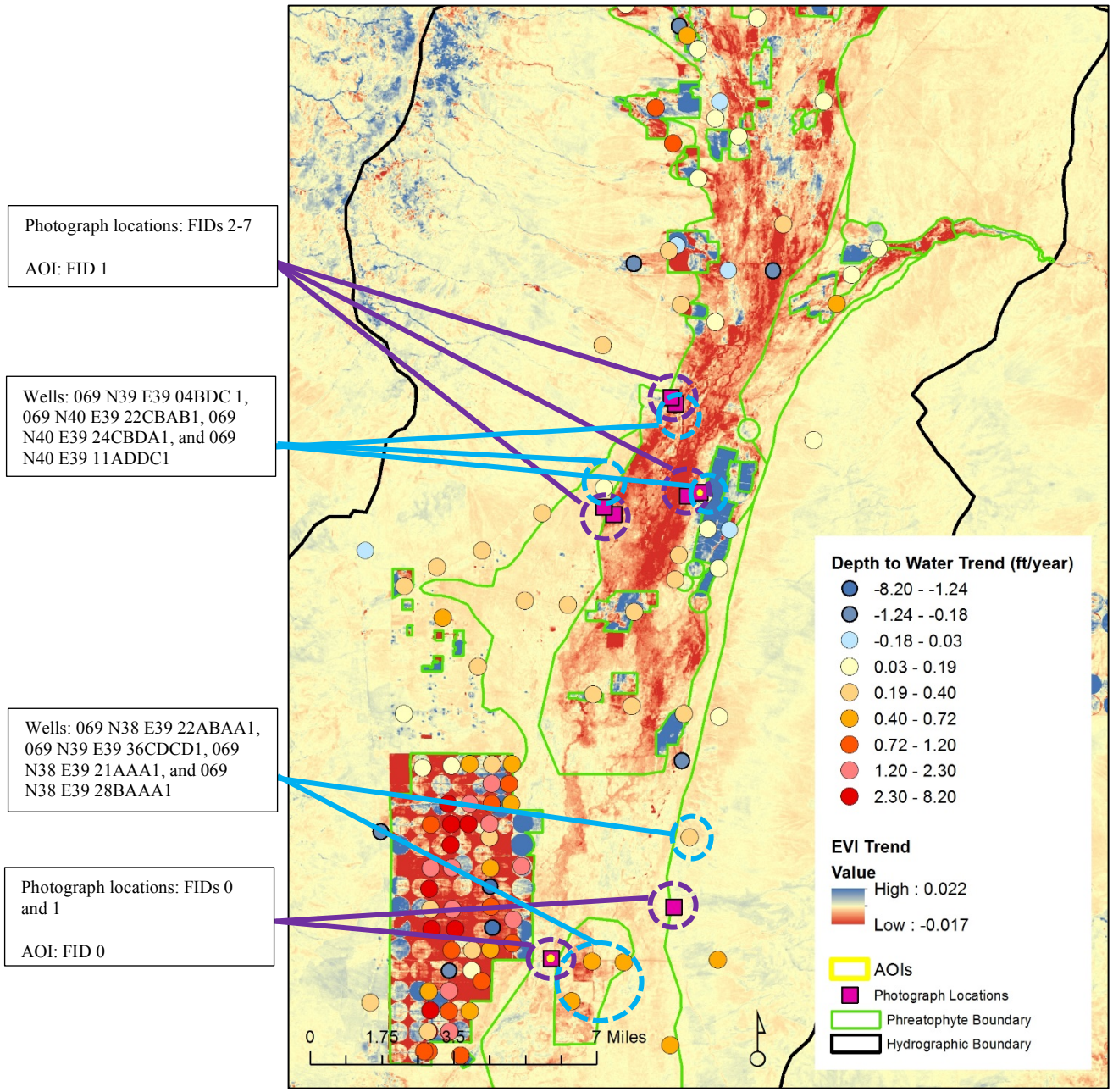


Figure 9. Paradise Valley (HA 69) groundwater level and EVI trends, site photograph locations, and AOIs.

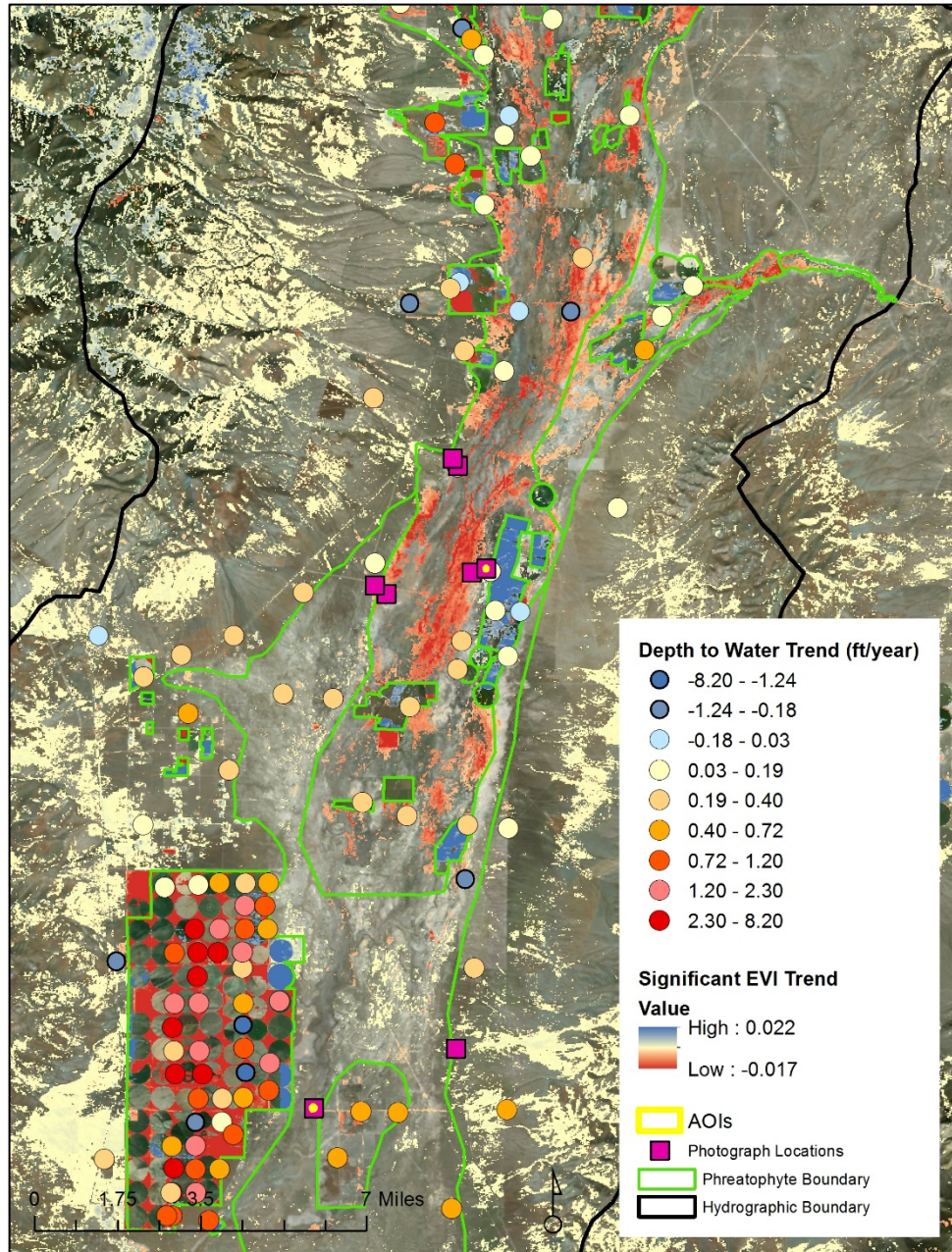


Figure 10. Paradise Valley (HA 69) groundwater level and EVI trends, site photograph locations, and AOIs. EVI trend pixels were masked out if p-values were greater than 0.10.

groundwater discharge area have increased by five feet since 1991 (Appendix 1-11; hydrographs for wells 069 N39 E39 04BDC 1; 069 N40 E39 22CBAB1; 069 N40 E39 11ADDC1). Interannual EVI values for AOIs associated with photo locations do not illustrate departure from water year PPT (Appendix 1-9 and 1-11; AOI FIDs 0 and 1).

Grass Valley (HA 71)

Trends in EVI and DTW at each well along with field-investigation photograph locations and phreatophyte boundaries are shown in Figures 11 and 12. Phreatophyte shrubland communities are composed primarily of greasewood, rabbitbrush, sagebrush, and saltgrass. Some buffalo berry was present in the central part of the basin. A moderately dense community of greasewood and rabbitbrush occupies an area just north and west of the primary irrigated area, and decreasing trends in vegetation vigor are evident in Figures 11 and 12. The greasewood within this area does not show signs of stress, however, rabbitbrush in this same area shows more signs of stress with some mortality (Appendix 1-12; photograph location (FID 0 and 1); photographs (pc_number 511 and 512)). Buffalo berry near this central part of the basin showed signs of stress and mortality (Appendix 1-12; photograph locations (FIDs 1-4); photographs (pc_number 513-515)). A monoculture of rabbitbrush north of this area appears to be stressed (Appendix 1-12; photograph location (FID 5); photographs (pc_number 517 and 518)), and a monoculture of greasewood along the east-central part of the groundwater discharge boundary shows signs of stress (Appendix 1-12; photograph location (FID 7); photograph (pc_number 520)). The DTW at the irrigated areas south of this region has increased from roughly 20 to 40 ft since 1992 (Appendix 1-12; hydrograph for well 071 N33 E37 13DDCB1). A community of greasewood with lesser amounts of rabbitbrush and sagebrush was present at the northern part of HA, and greasewood appeared to be the only stressed vegetation in the area (Appendix 1-13; photograph locations (FID 8 and 9); photographs (pc_number 546-556)). DTW at the irrigated areas just north of the site has increased from 30 to 50 ft since 1991 (Appendix 1-13; hydrograph for well 071 N35 E37 36BDCB1). Interannual EVI values for AOIs associated with photograph locations do not illustrate departure from water year PPT (Appendix 1-12 and 1-13; AOI FIDs 0-2), with the exception of one, which indicates a fairly consistent decline and departure from water year PPT beginning in 2013 (Appendix 1-12; AOI FID 3). This area is located in the central part of the discharge area and north of the primary irrigated area, and is associated with observed rabbitbrush mortality (Appendix 1-12; photograph location (FID 5); photographs (pc_number 517 and 518)).

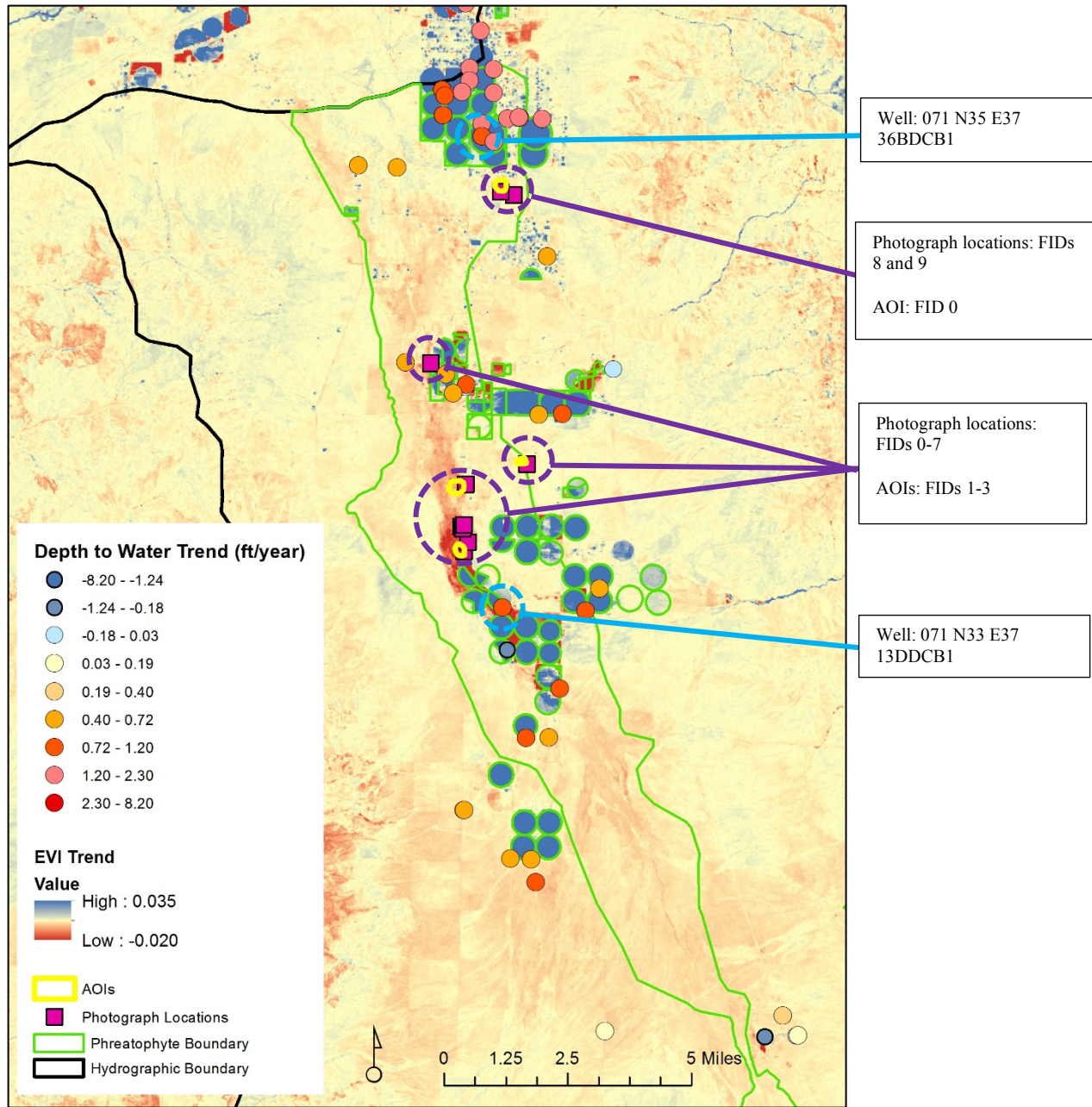


Figure 11. Grass Valley (HA 71) groundwater level and EVI trends, site photograph locations, and AOIs.

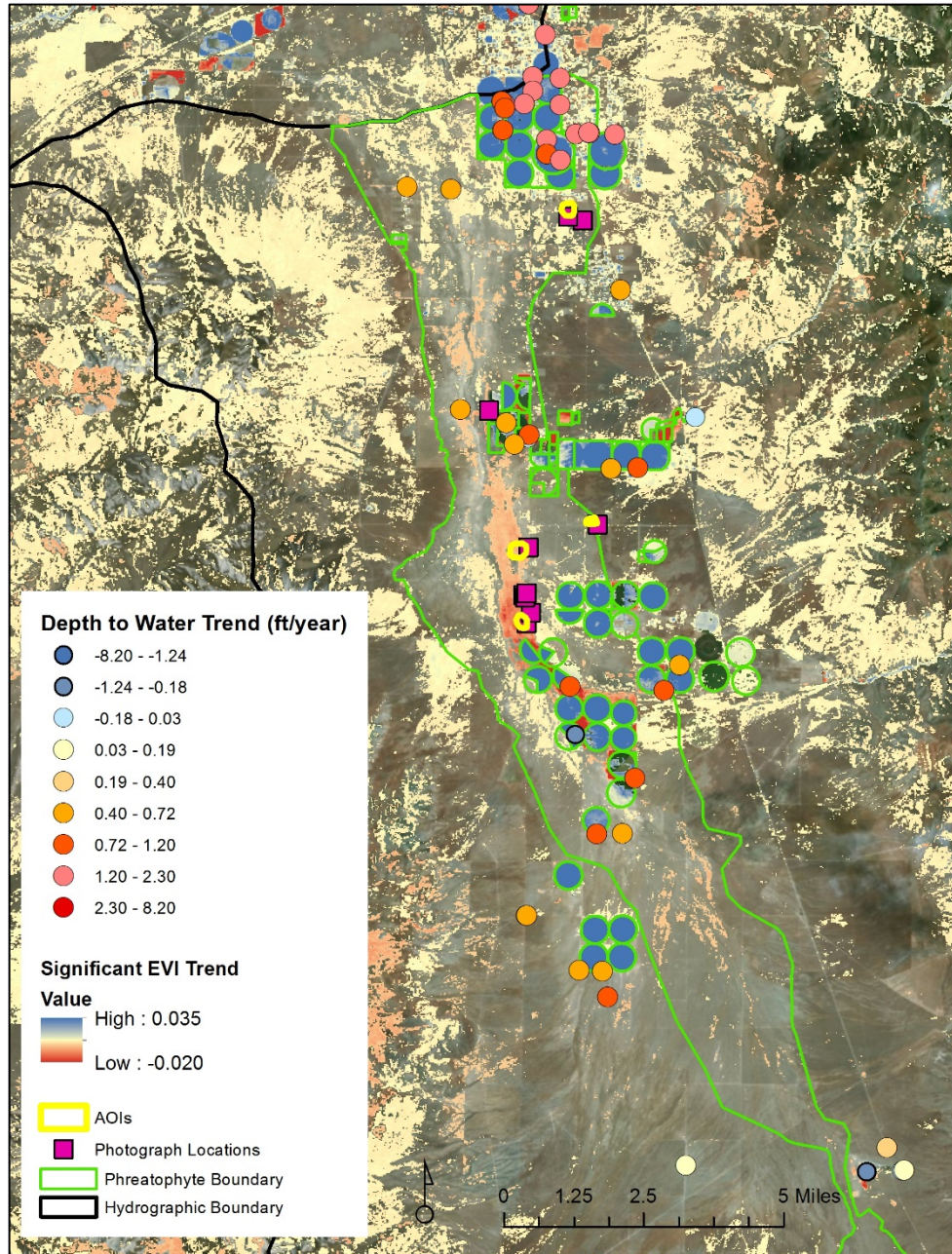


Figure 12. Grass Valley (HA 71) groundwater level and EVI trends, site photograph locations, and AOIs. EVI trend pixels were masked out if p-values were greater than 0.10.

Edwards Creek Valley (HA 133)

Trends in EVI along with field-investigation photograph locations and phreatophyte boundaries are shown in Figures 13 and 14. Phreatophyte shrubland communities are composed of greasewood, rabbitbrush, sagebrush, and shadscale. A moderately dense community of sagebrush and rabbitbrush southwest of the playa shows signs stress (Appendix 1-14; photograph location (FID 0); photographs (pc_number 420-423)). Slightly west of this site is a community of greasewood, sagebrush, and shadscale; all of the shrubs show signs of stress and even mortality (Appendix 1-14; photograph location (FID 0); photographs (pc_number 424-429)). DTW in this area is unknown (although it is presumed to be < 30ft) and no known groundwater pumping has occurred nearby or within a reasonable distance that would increase DTW in the area (see Google Earth Engine time lapse - <https://goo.gl/Bgczyl>).

DISCUSSION and CONCLUSIONS

Findings from this study illustrate that phreatophyte vegetation vigor changes can be observed from remotely sensed satellite imagery, and confirmed with field investigations. While localized phreatophyte vegetation stress and mortality was assumed to be attributed to increased DTW due to groundwater pumping, stress and mortality was not widespread, making this assumption questionable without consideration of numerous other factors. Localized stress and mortality can occur for reasons other than increased DTW, such as drought, disease, and land management (e.g., grazing, herbicides, and land clearing). Separating these factors is difficult; however, where DTW has increased and there are clear signs of phreatophyte stress or mortality and absence of other factors (e.g., drought, grazing), the likelihood that groundwater pumping and capture of phreatophyte ET is the cause of such localized stress and/or mortality is high (Huntington et al., 2016). Also, a combination of these factors would likely increase the risk of local and/or regional stress and mortality.

A common observation where localized stress and mortality was observed was that greasewood seemed to show little to no signs of stress. This is likely due to the fact that greasewood has been documented to have deeper root structure than sagebrush and rabbitbrush, and is generally more resistant to drought and other environmental stressors due to its ability to shed leaves and sections of canopy during moisture stress (Lei 1999; Robertson, 1983). Observations of mixed impacts from this study are similar to previously reported findings in which increased DTW in Owens Valley, CA resulted in decreased phreatophyte vegetation vigor for some but not all sites (Sorenson et al., 1989; 1991). Results found in the current study contrast with findings from a study in the San Luis Valley, CO, where extensive groundwater pumping has increased DTW, and greasewood was affected by increased DTW, but rabbitbrush was not, as determined by differences in relative ET measurements (Charles, 1987). Cooper (2006) concluded that the wide range

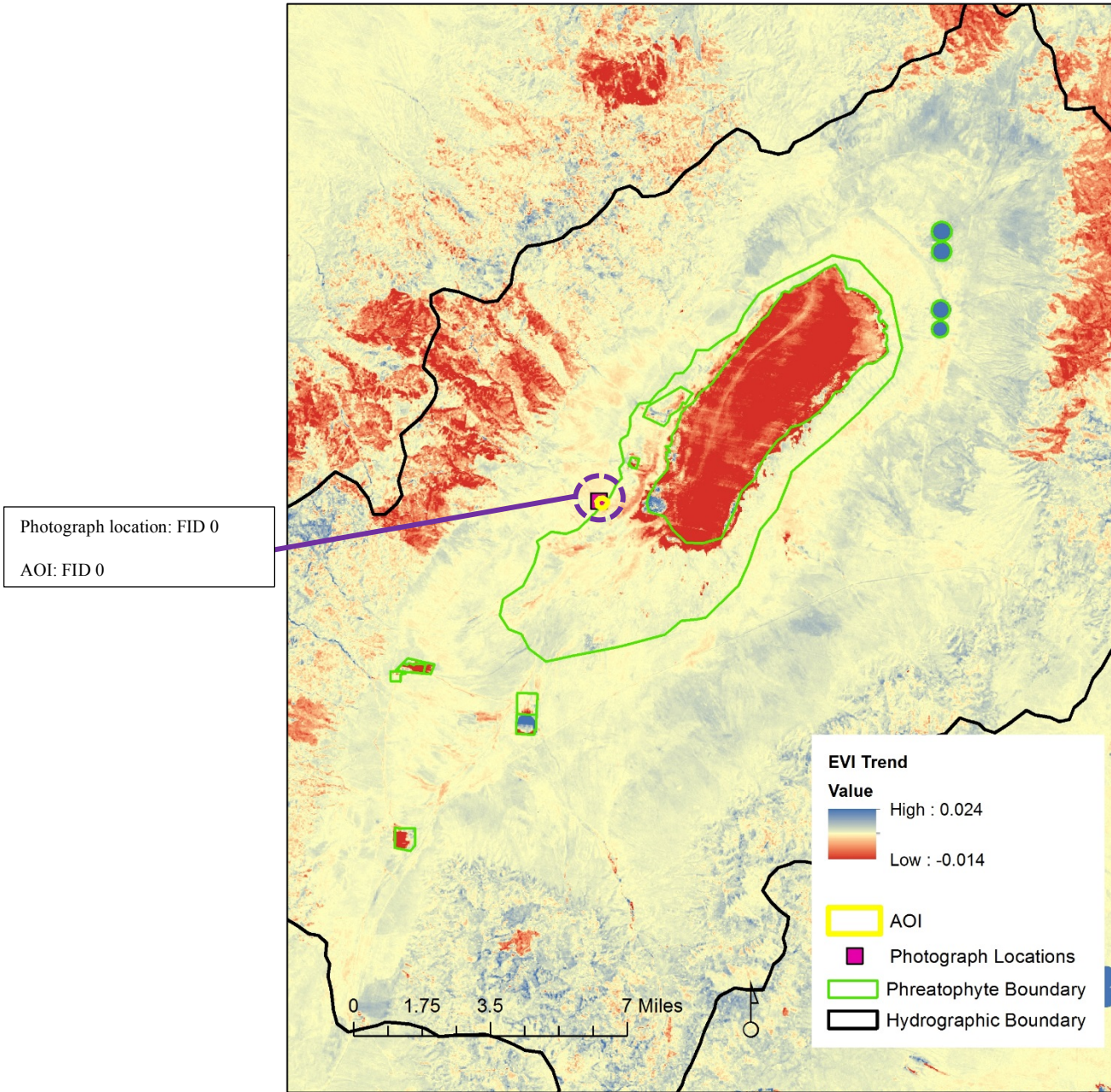


Figure 13. Edwards Creek Valley (HA 133) EVI trends, site photograph locations, and an AOI.

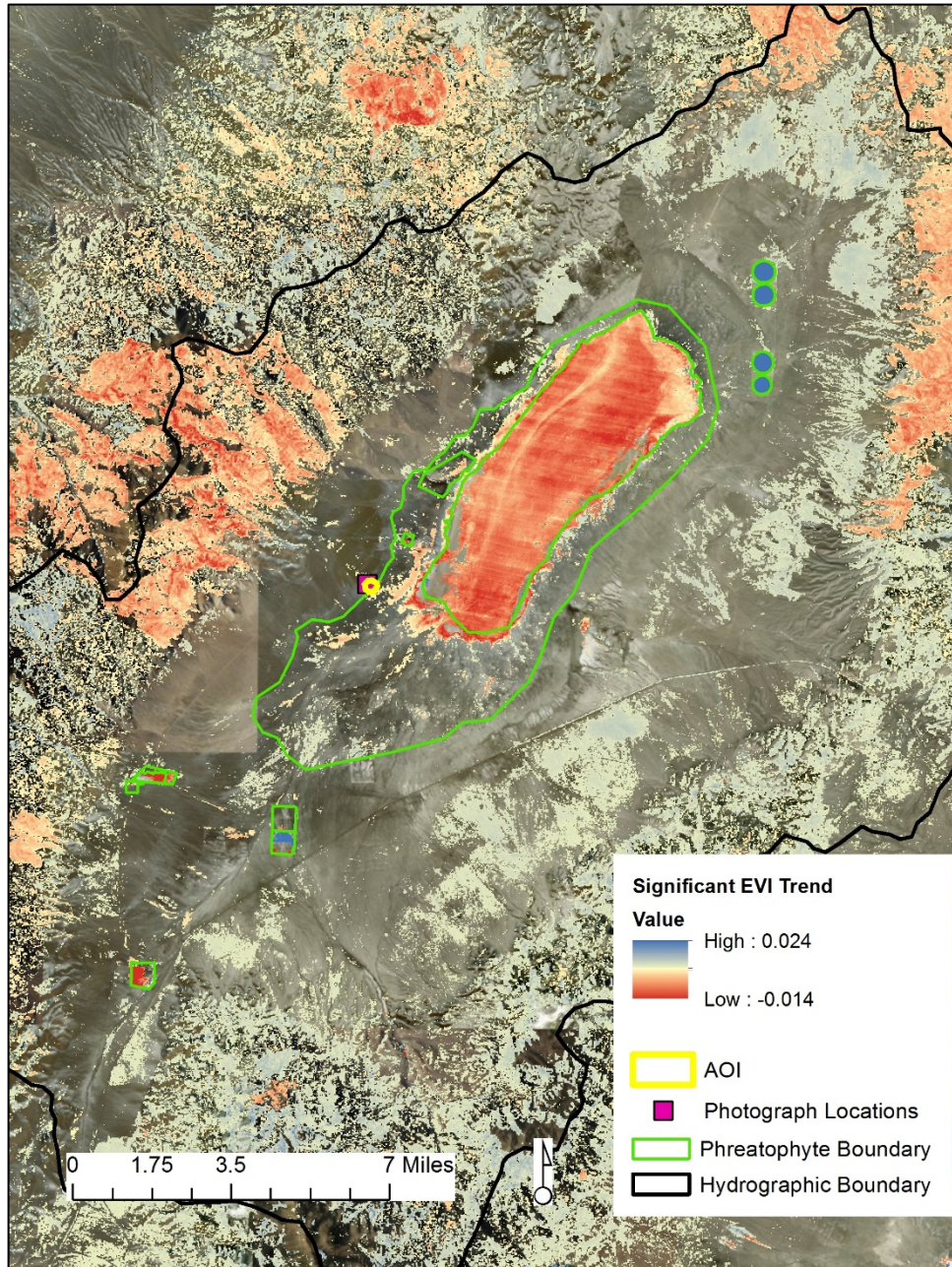


Figure 14. Edwards Creek Valley (HA 133) EVI trends, site photograph locations, and an AOI. EVI trend pixels were masked out if p-values were greater than 0.10.

of reported impacts and response times could be due to the fact that greasewood can regulate seasonal uptake of shallow precipitation derived soil water vs. deeper groundwater and can grow deeper roots as the DTW increases, whereas rabbitbrush can survive without access to groundwater.

An important conclusion from this study is that while declines in EVI and localized stress and mortality was observed, facultative phreatophyte vegetation persists within groundwater discharge areas where DTW was historically at or near land surface (i.e., 0 to 30 ft) and currently exceeds typically reported range of rooting depths (~20 to 60 ft). For the HAs studied in this report, increases in DTW are due to groundwater pumping for irrigation, and the rate of change in DTW is variable depending on the basin and location within. The rate of change in DTW is thought to be a primary factor in determining the degree of phreatophyte stress and potential plant succession (Naumburg et al., 2005). Other factors such as soil type, soil salinity, permeability, and climate are also important. Mean annual PPT within phreatophyte areas investigated in this study ranges from 8 to 10 inches per year, and on average, may be enough to sustain facultative phreatophyte vegetation in the absence of shallow groundwater. However, sustained periods of drought and higher than average evaporative demand may stress phreatophytes to the point of mortality. Based on long term and continuous historical pumping and resulting DTW increases within phreatophyte areas documented in 1960s reconnaissance series reports and water resources bulletins, along with results from field investigations during this study, it is hypothesized that mortality would likely be localized and/or species specific if DTW increased during extensive drought periods. Ideally, primary factors that control phreatophyte states and potential transitions would be well known and defined, and the use of ecological dynamics simulation models such as EDYS or customized state and transition models specific for phreatophyte vegetation could be used to address and predict vegetation response to water table fluctuations. However, at this time, the basic information needed to define model parameters and state and transition thresholds are not well known or defined. Detailed literature reviews, additional observations and field investigations, and additional research on this topic is desperately needed, but beyond the scope of this initial reconnaissance study focused on spatiotemporal distributions of phreatophyte vegetation vigor within selected HAs in Nevada.

FUTURE WORK

Expanding the trend analyses implemented in this study to more HAs would be useful for developing a robust database documenting spatiotemporal patterns of phreatophyte vegetation vigor. Disentangling the impacts on GDEs caused by variations in climate and hydrology vs. land management is necessary as monitoring, management, and mitigation plans are proposed and developed. Including more HAs with past groundwater development in an analysis similar to this study would be useful to further document vegetation vigor

change that may have resulted from changes in available groundwater. On the other hand, performing a similar analysis for HAs where there has been no groundwater development would be useful to establish baseline trends, and determine if natural variability and other management factors are driving GDE changes. For example, taking into account confounding variables like grazing history, fire history, and invasive species encroachment will assist in determining causality of change. Reviewing historical reports that contain information about historical vegetation composition, and comparing that composition to current vegetation composition would be helpful for determining if plant succession has already occurred.

Prior to field site visits, locating impacted GDEs with Landsat and conducting detailed historical research and data analyses in the office will be important to establish a more thorough understanding of field site conditions, as well as saving time in the field once at the site. Identifying and focusing on sites with ample groundwater level data, vegetation, fire, and grazing history, soils information, and vegetation change within the Landsat archive will help better prepare for site visits and data interpretation. Ideally, three to four interdisciplinary teams of two people each would conduct an intensive field campaign in mid- to late-summer after detailed research and data preparation is conducted in the office. During office preparation and field work, collaboration with plant ecologists and/or range specialists is needed to improve the study. While our team is well versed in hydrology and remote sensing of vegetation, any future study would greatly benefit from having plant ecologists and/or range specialists that have detailed knowledge of plant physiology for common phreatophyte communities found in the Great Basin.

The statistical analysis could be improved by conducting regression analyses between annual vegetation indices and PPT at the pixel level to statistically determine relationships between these two variables. This is likely to assist with better understanding the sensitivity of GDEs to climate variability, and help to separate natural vs management caused sensitivity. Another consideration for statistical improvement is to address autocorrelation of EVI and PPT time series at the pixel level; possible approaches include a per-pixel Durbin-Watson test and the use of an ARIMA model.

REFERENCES

- Abatzoglou, J.T. (2013). Development of gridded surface meteorological data for ecological applications and modeling. *International Journal of Climatology*.
DOI:10.1002/joc.3413
- Albright, W. R. Jasoni, M. Cablk, J. Thomas, D. Decker, & J. Arnone. (2006).
Evapotranspiration in Smoke Creek Desert, Nevada. Desert Research Institute,
Division of Hydrologic Sciences Publication No. 41224.
- Allander, K.K., J.L. Smith, & M.J. Johnson (2009). Evapotranspiration from the lower
Walker River basin, west-central Nevada, water years 2005–07, U.S. Geol. Sur. Sci.
Invest. Rep. 2009-5079, 62 pp.
- ASCE-EWRI (2005). The ASCE Standardized Reference Evapotranspiration Equation.
ASCE-EWRI Standardization of Reference Evapotranspiration Task Committee
Report, available at <http://www.kimberly.uidaho.edu/water/asceewri/>
- Beamer, J., J.L. Huntington, C. Morton, & G. Pohll (2013). Estimation of annual
groundwater evapotranspiration from phreatophyte vegetation in the Great Basin
using remotely sensed vegetation indices and ground based flux tower measurements.
Journal of the American Water Resources Association, 49(3), 518-533.
DOI:10.1111/jawr.12058
- Box G, Jenkins G. 1970. *Time Series Analysis: Forecasting and Control*. San Francisco:
Holden-Day.
- Bredehoeft, J. D. (2002). The water budget myth revisited: why hydrogeologists
model. *Groundwater*, 40(4), 340-345.
- Charles, F.L., 1987. Evapotranspiration of phreatophytes in the San Luis Valley, Colorado.
MS Thesis. Colorado State University, Fort Collins, CO.
- Childress, W. M., & T. McLendon. 1999. Simulation of multi-scale environmental impacts
using the EDYS model. *Hydrological Science and Technology* 15:257–269.
- Childress, W. M. 1999. A multi-scale ecological model for allocation of training activities on
US army installations. Pages 80–108 in J. M. Klopatek (ed.), *Landscape ecological
analysis: Issues and applications*. Springer, New York.
- Childress, W. M., D. L. Price, C. L. Coldren, & T. McLendon. 1999. A functional description
of the ecological dynamics simulation (EDYS) Model, with applications for army and
other federal land managers. P CERL Technical Report 99/ 55. US Army Corps of
Engineers, Construction Engineering Research Laboratory, Champaign, Illinois, 68
pp.

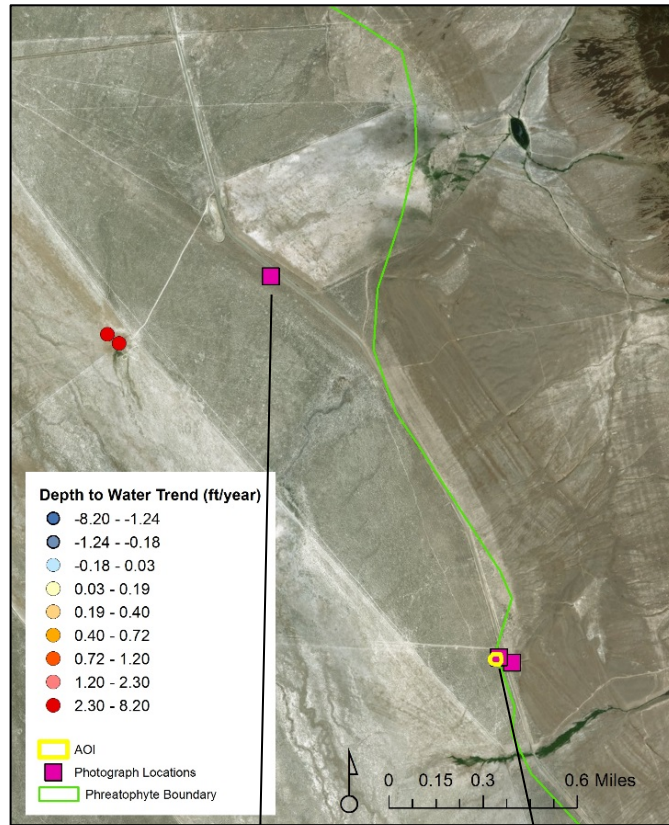
- Chimner, R. A., & Cooper, D. J. (2004). Using stable oxygen isotopes to quantify the water source used for transpiration by native shrubs in the San Luis Valley, Colorado USA. *Plant and Soil*, 260(1-2), 225-236.
- Cooper, D. J., Sanderson, J. S., Stannard, D. I., & Groeneveld, D. P. (2006). Effects of long-term water table drawdown on evapotranspiration and vegetation in an arid region phreatophyte community. *Journal of Hydrology*, 325(1-4), 21-34.
- Daly C, M. Halbleib, J.I. Smith, W.P. Gibson, M.K. Doggett, G.H. Taylor, J. Curtis, & P.A. Pasteris (2008). Physiographically-sensitive mapping of temperature and precipitation across the conterminous United States. *International Journal of Climatology*. DOI:10.1002/joc.1688
- Dawson, T. E., & Pate, J. S. (1996). Seasonal water uptake and movement in root systems of Australian phraeatophytic plants of dimorphic root morphology: a stable isotope investigation. *Oecologia*, 107(1), 13-20.
- Eakin, T., & D. Everett. (1965). *Water Resources Appraisal of the Upper Reese River Valley, Lander and Nye Counties, Nevada*. Water Resources Reconnaissance Series Report 31, 47 p.
- Elmore, A.J., Mustard, J.F. & Manning, S.J., 2003. Regional patterns of plant community response to changes in water: Owens Valley, California. *Ecological Applications*, 13(2), pp.443-460.
- Garcia, C.A., Huntington, J.M., Buto, S.G., Moreo, M.T., Smith, J.L., & Andraski, B.J., (2015), *Groundwater discharge by evapotranspiration, Dixie Valley, west-central Nevada, March 2009–September 2011 (ver. 1.1, April 2015)*: U.S. Geological Survey Professional Paper 1805, 90 p., <http://dx.doi.org/10.3133/pp1805>.
- Glancy, P. A., & Eugene R. (1968). *Water-Resources Appraisal of Smoke Creek-San Emidio Desert Area, Nevada and California*. Nevada Department of Conservation and Natural Resources, Water Resources-Reconnaissance Series Report, 55 p.
- Gorelick, N., Hancher, M., Dixon, M., Ilyushchenko, S., Thau, D., & Moore, R. (2017). Google Earth Engine: Planetary-scale geospatial analysis for everyone. *Remote Sensing of Environment*, 202, 18-27.
- Groeneveld, D.P., W.M. Baugh, J.S. Sanderson, & D.J. Cooper (2007). Annual groundwater evapotranspiration mapped from single satellite scenes. *Journal of Hydrology*, 344, 146-156. DOI:10.1016/j.jhydrol.2007.07.002
- Groeneveld, D. P. (2008). Remotely-sensed groundwater evapotranspiration from alkali scrub affected by declining water table. *Journal of hydrology*, 358(3-4), 294-303.
- Helsel, D.R., Hirsch, R.M., 1992. *Statistical methods in water resources*. 49. Elsevier

- Huete, A., Didan, K., Miura, T., Rodriguez, E. P., Gao, X., & Ferreira, L. G. (2002). Overview of the radiometric and biophysical performance of the MODIS vegetation indices. *Remote sensing of environment*, 83(1-2), 195-213.
- Huxel, C.J. (1966). Effects of Irrigation Development on the Water Supply of Quinn River Valley Area, Nevada and Oregon, 1950-64. State of Nevada, Department of Conservation and Natural Resources, Water Resources Bulletin 34.
- Huntington, J., McGwire, K., Morton, C., Snyder, K., Peterson, S., Erickson, T., ... & Allen, R. (2016). Assessing the role of climate and resource management on groundwater dependent ecosystem changes in arid environments with the Landsat archive. *Remote sensing of Environment*, 185, 186-197.
- Lei, S. A. 1999. Effects of severe drought on biodiversity and productivity in a creosote bush-blackbrush ecotone of southern Nevada. In D. E. McArthur, K. W. Ostler, C. L. Wambolt [eds.] *Proceedings: shrubland ecotones*. RMRS-P-11. U.S. Department of Agriculture, Forest Service, Rocky Mountain Research Station, Ephraim, UT. p. 217-221
- Malmberg G.T. & G.F. Worts. (1966). The Effects of Pumping on the Hydrology of Kings River Valley, Humboldt County, Nevada, 1957-64. State of Nevada, Department of Conservation and Natural Resources, Water Resources Bulletin 31, 53 p.
- Mitchell K.E., D. Lohmann, P.R. Houser, Wood E.F., J.C. Schaake, A. Robock, B.A. Cosgrove, J. Sheffield, Q. Duan, L. Luo, R.W. Higgins, R.T. Pinker, J.D. Tarpley, D.P. Lettenmaier, C.H. Marshall, J.K. Entin, M. Pan, W. Shi, V. Koren, J. Meng, B.H. Ramsay, and A.A. Bailey (2004). The multi-institution North American Land Data Assimilation System (NLDAS): Utilizing multiple GCIP products and partners in a continental distributed hydrological modeling system. *Journal of Geophysical Research*, 109, D07S90. DOI:10.1029/2003JD003823
- Naumburg, E., Mata-Gonzalez, R., Hunter, R. G., Mclendon, T., & Martin, D. W. (2005). Phreatophytic vegetation and groundwater fluctuations: a review of current research and application of ecosystem response modeling with an emphasis on Great Basin vegetation. *Environmental Management*, 35(6), 726-740.
- Nichols, W.D. (2000). Regional groundwater evapotranspiration and groundwater budgets, Great Basin, Nevada. U.S. Geological Survey Professional Paper 1628, 82 pp.
- Patten, D. T., Rouse, L., & Stromberg, J. C. (2008). Isolated spring wetlands in the Great Basin and Mojave Deserts, USA: potential response of vegetation to groundwater withdrawal. *Environmental Management*, 41(3), 398-413.
- Robertson, J. (1983). Greasewood (*Sarcobatus vermiculatus* (Hook.) Torr.). *Phytologia* 54:309-324.

- Robinson, T.W. (1958). Phreatophytes, U.S. Geol. Sur. Water Sup. Pap., 1423, 84pp.
- Schmidt, G., Jenkerson, C., Masek, J., Vermote, E., & Gao, F. (2013). Landsat ecosystem disturbance adaptive processing system (LEDAPS) algorithm description (No. 2013-1057). US Geological Survey.
- Sorenson, S.K., Dileanis, P.D., Branson, F.A. (1989). Soil water and vegetation responses to precipitation and changes in depth to ground water in Owens Valley, California. US Geological Survey Open-file Report 89-260.
- Sorenson, S.K., Dileanis, P.D., Branson, F.A. (1991). Soil water and vegetation responses to precipitation and changes in depth to ground water in Owens Valley, California. US Geological Survey Water-Supply Paper 2370.
- Stromberg, J.C., Tiller, R. and Richter, B., 1996. Effects of groundwater decline on riparian vegetation of semiarid regions: the San Pedro, Arizona. *Ecological Applications*, 6(1), pp.113-131.
- U.S. Geological Survey. (2018). Landsat 8 Surface Reflectance Code (LaSRC) Product, version 4.3, March 2018., 40 p.
- Zones C.P. (1963). Ground Water in the Alluvium of Kings River Valley Humboldt County, Nevada. Geological Survey Water Supply Paper 1619-L, Water Resources Bulletin 16, 38p.
- Zhu, Z., & Woodcock, C. E. (2012). Object-based cloud and cloud shadow detection in Landsat imagery. *Remote sensing of environment*, 118, 83-94.

APPENDIX 1 – Select Site Photographs and Well Hydrographs.

Appendix 1-1. Kings River Valley (HA 30A) Close-up, Site Photographs, Well Hydrographs, and AOI EVI-PPT Graphs for Eastern Part of the Valley



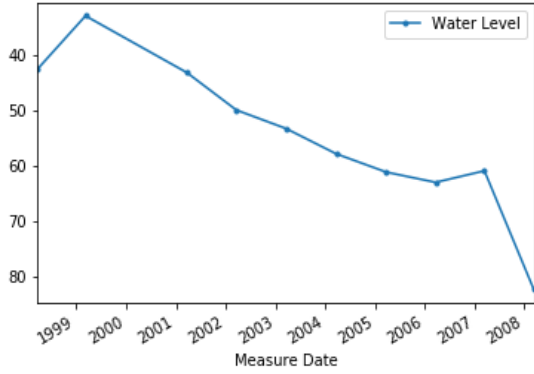
Close-up view of well locations (030A N45 E34 29ABBC1 and 030A N45 E34 29ABBC2), photograph locations (FIDs 2-4), and an AOI (FID 2) (note: AOI FID 3 is out of view to the north-west in the close-up).



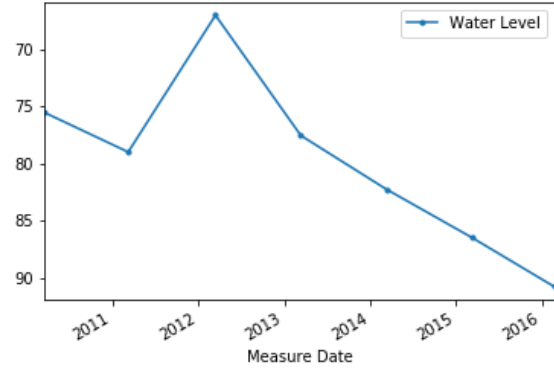
Northwest facing photograph (pc_number 526).



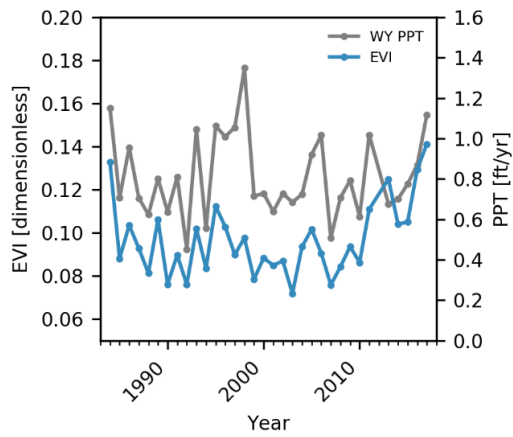
Southwest facing photograph (pc_number 528; AOI FID 2).



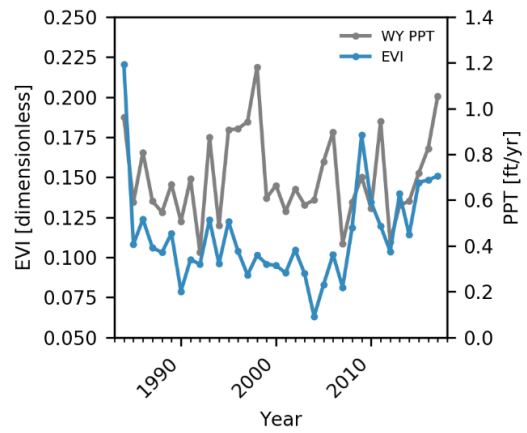
Well hydrograph (feet below surface): 030A N45 E34 29ABBC1.



Well hydrograph (feet below surface): 030A N45 E34 29ABBC2.

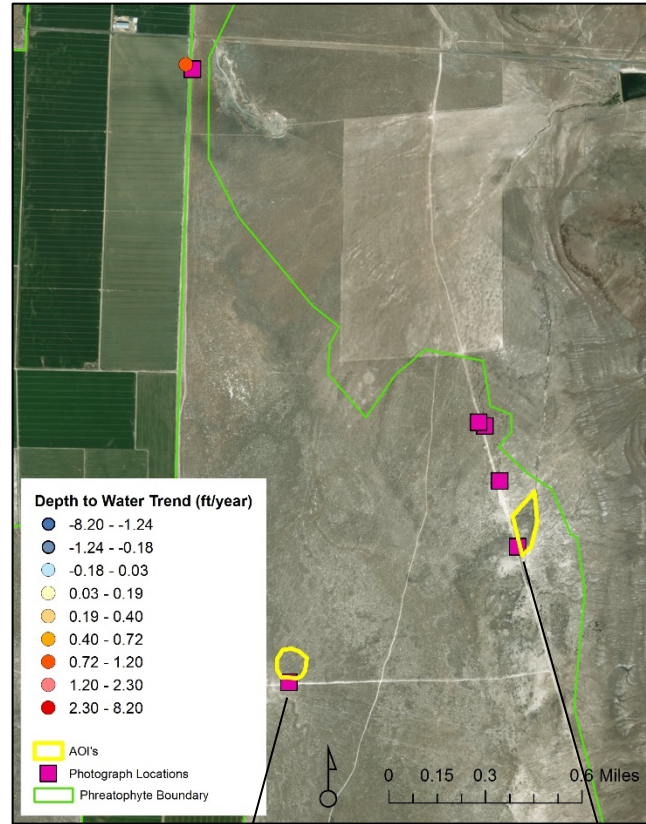


EVI and PPT for AOI (FID 2).



EVI and PPT for AOI (FID 3).

Appendix 1-2. Kings River Valley (HA 30A) Close-up, Site Photographs, Well Hydrographs, and AOI EVI-PPT Graphs for South-Eastern part of the Valley



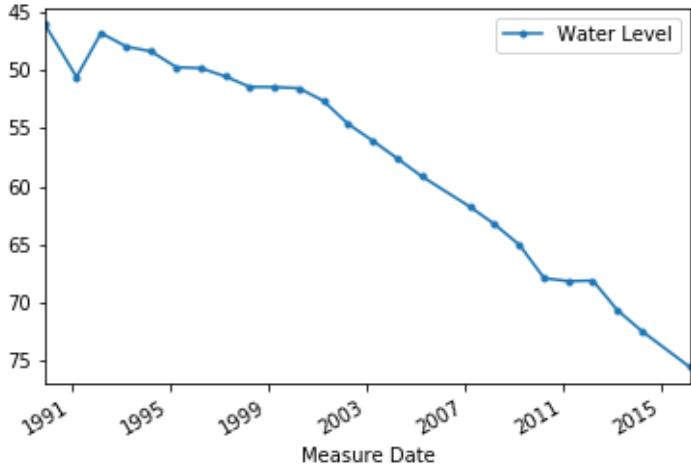
Close-up view of well location (030A N44 E34 16AAA1), photograph locations (FIDs 11-15), and AOIs (FIDs 0 and 1).



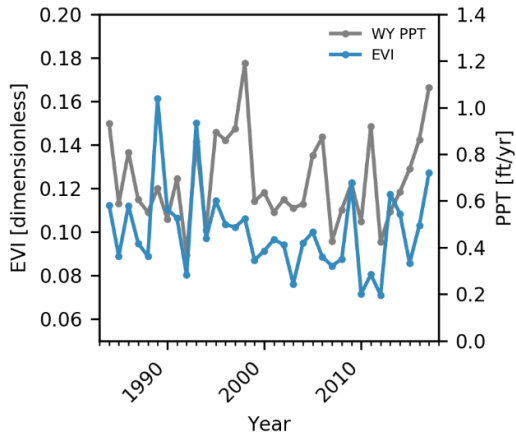
Northeast facing photograph (pc_number 541; AOI FID 1).



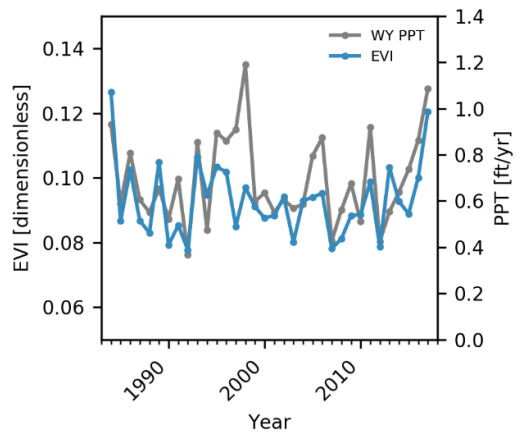
East facing photograph (pc_number 542; AOI FID 0).



Well hydrograph (feet below surface): 030A N44 E34 16AAAA1.

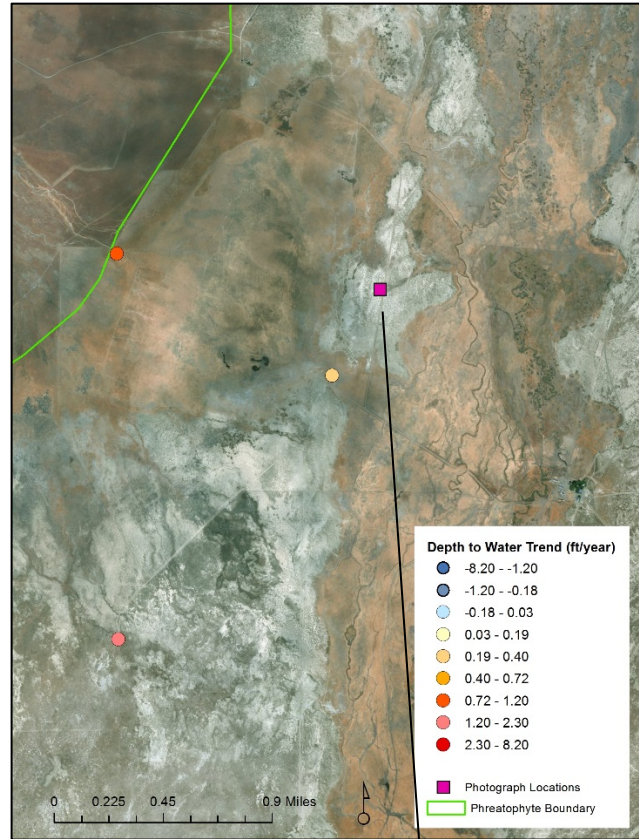


EVI and PPT for AOI (FID 0).



EVI and PPT for AOI (FID 1).

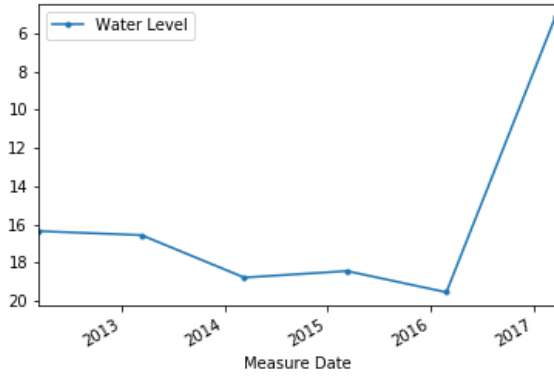
Appendix 1-3. Quinn River Valley (HA 33A) Close-up, Site Photograph and Well Hydrographs for North-Central part of the Valley



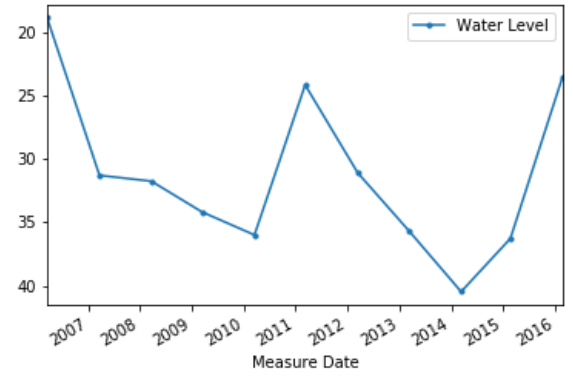
Close-up view of well locations (033A N44 E36 26ACB1, 033A N44 E36 22DCAA1, 033A N44 E36 34ADBC1) and photograph location (FID 0).



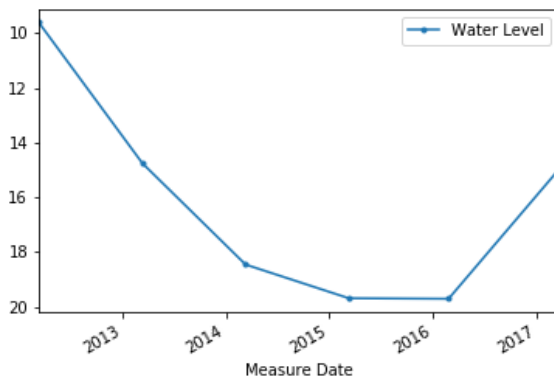
East facing photograph (pc_number 521).



Well hydrograph (feet below surface): 033A N44 E36 26ACB1.

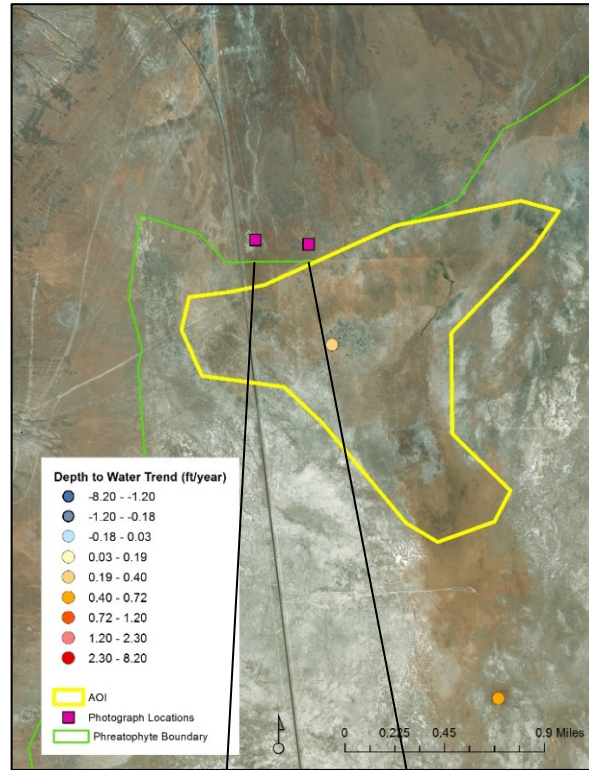


Well hydrograph (feet below surface): 033A N44 E36 22DCAA1.



Well hydrograph (feet below surface): 033A N44 E36 34ADBC1.

Appendix 1-4. Quinn River Valley (HA 33A) Close-up, Site Photographs, Well Hydrographs, and AOI EVI-PPT Graph for North-Western part of the Valley



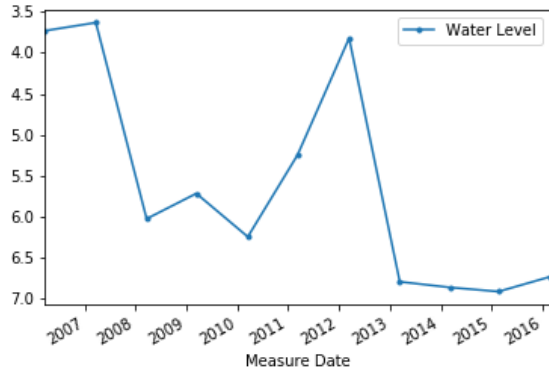
Close-up view of well locations (033A N44 E36 33BCDA1; 033A N43 E36 04DDDD1), photograph locations (FIDs 1 and 2), and an AOI (FID 0).



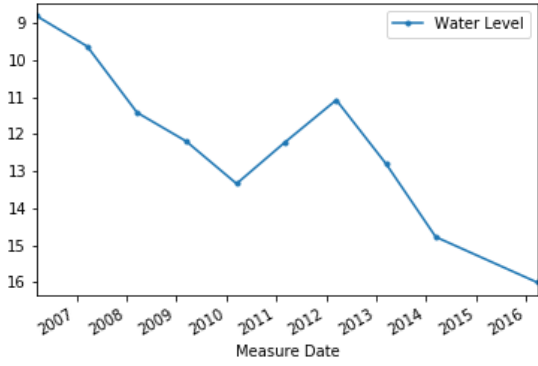
East facing photograph (pc_number 522; AOI FID 0).



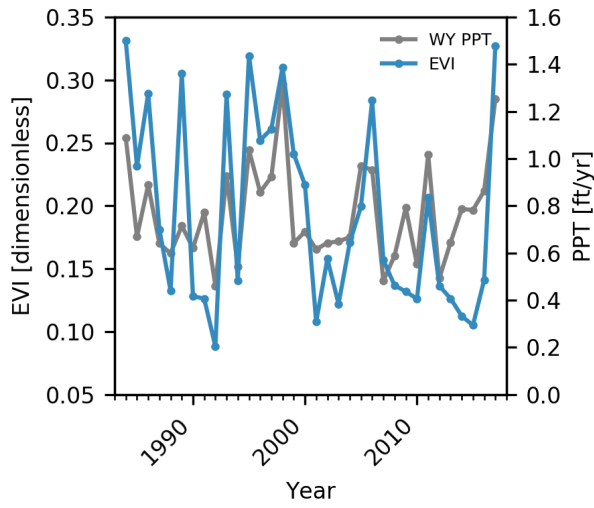
East facing photograph (pc_number 523; AOI FID 0).



Well hydrograph (feet below surface): 033A N44 E36 33BCDA1.

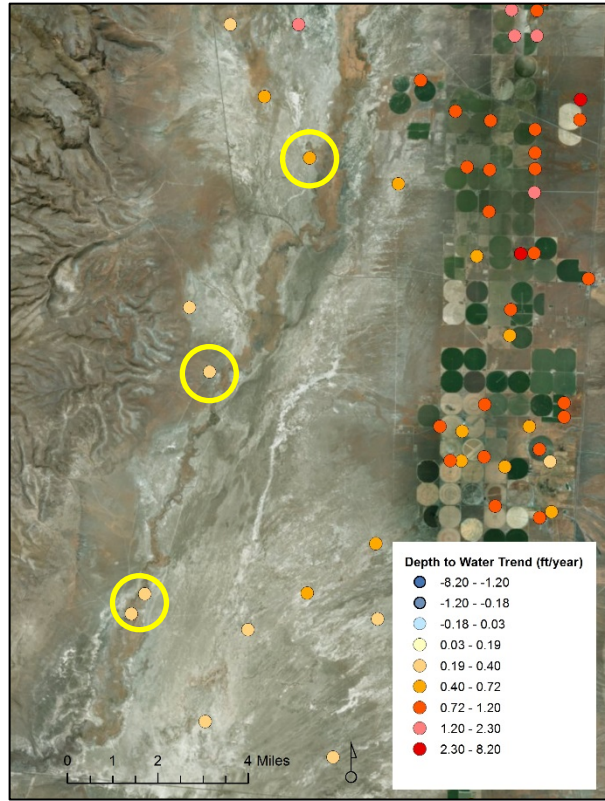


Well hydrograph (feet below surface): 033A N43 E36 04DDDD1.

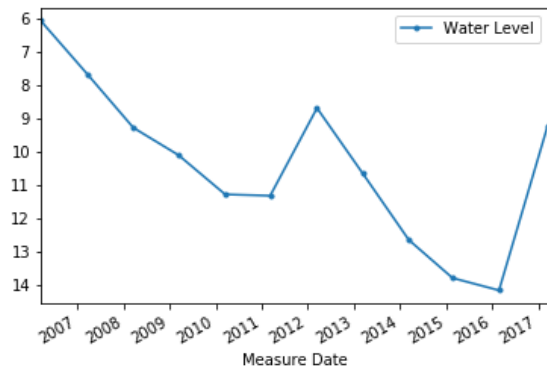


EVI and PPT for AOI (FID 0).

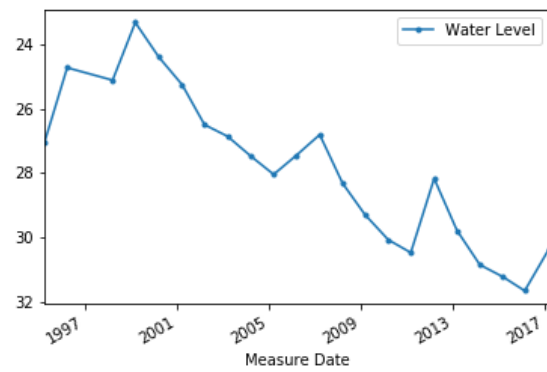
Appendix 1-5. Quinn River Valley (HA 33A) Close-up and Hydrographs for Wells along the Quinn River



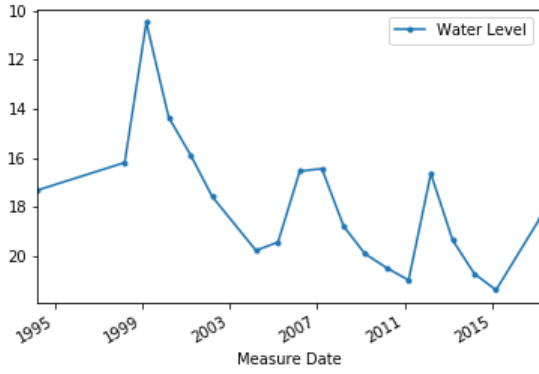
Close-up view of well locations (033A N43 E36 14BCBB1; 033A N42 E36 08AAB 1; 033A N41 E36 06ABBB1; 033A N41 E36 06CBAA1). Wells of interest are within yellow circles on map.



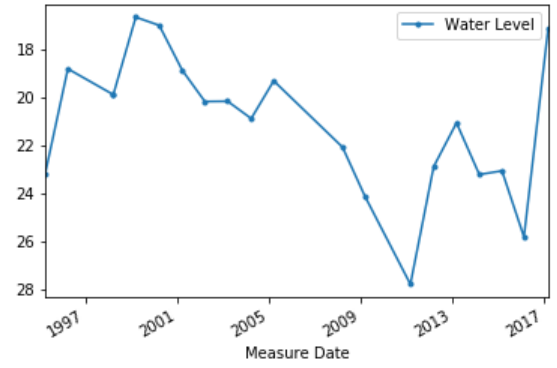
Well hydrograph (feet below surface): 033A N43 E36 14BCBB1.



Well hydrograph (feet below surface): 033A N42 E36 08AAB1.

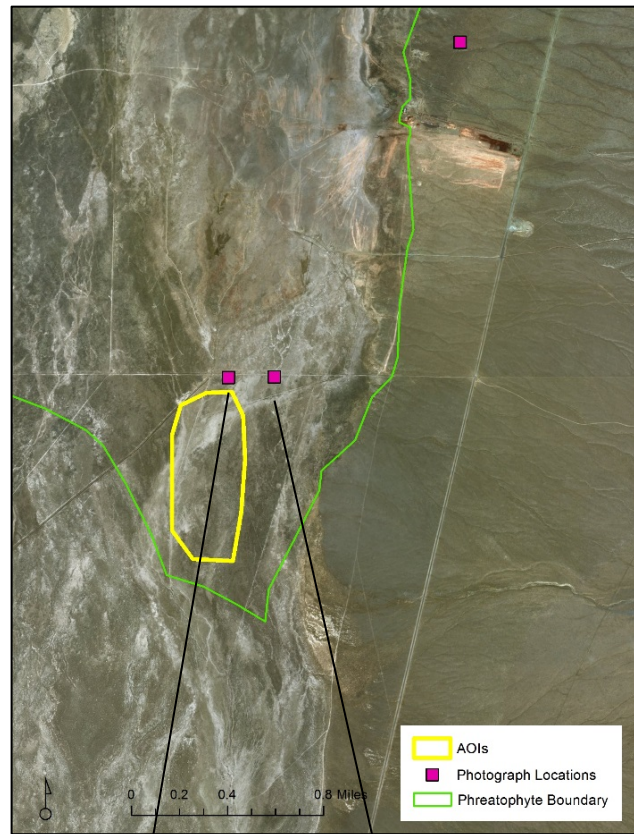


Well hydrograph (feet below surface): 033A N41 E36 06ABB1.



Well hydrograph (feet below surface): 033A N41 E36 06CBAA1.

Appendix 1-6. Upper Reese River Valley (HA 56) Close-up, Site Photographs, and AOI EVI-PPT Graph for Southern Part of the Valley



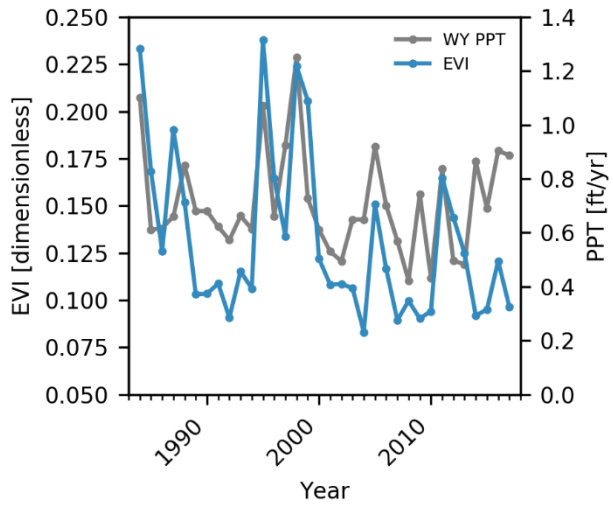
Close-up view of photograph locations (FIDs 0 and 1) and an area of interest (FID 0).



South facing photograph (pc_number 430; AOI FID 0).



East facing photograph (pc_number 455).



EVI and PPT for AOI (FID 0).

Appendix 1-7. Upper Reese River Valley (HA 56) Close-up and Site Photographs for the Eastern Part of the Valley

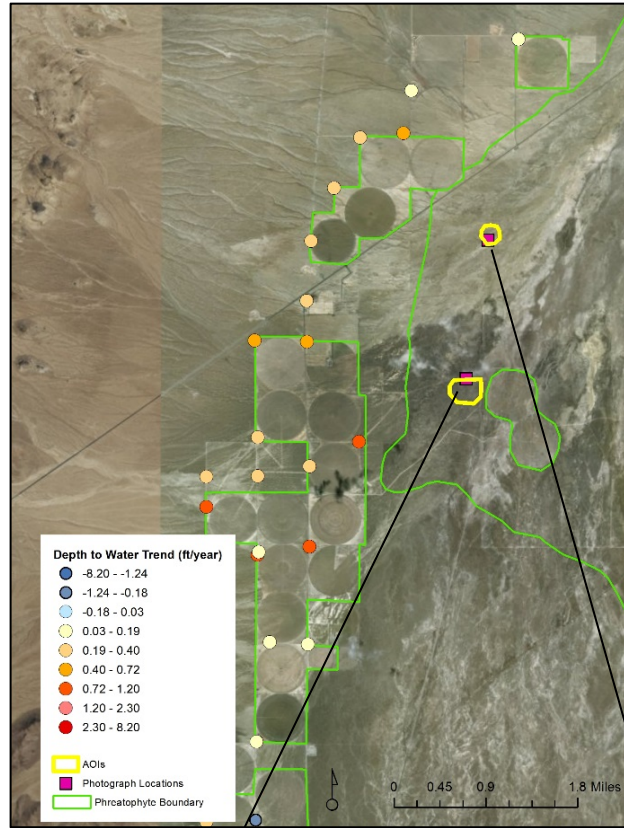


Close-up view of photograph locations (FIDs 2 and 3).



West facing photograph (pc_number 474).

Appendix 1-8. Upper Reese River Valley (HA 56) Close-up, Site Photographs, Well Hydrographs, and AOI EVI-PPT Graphs for Western Part of the Valley



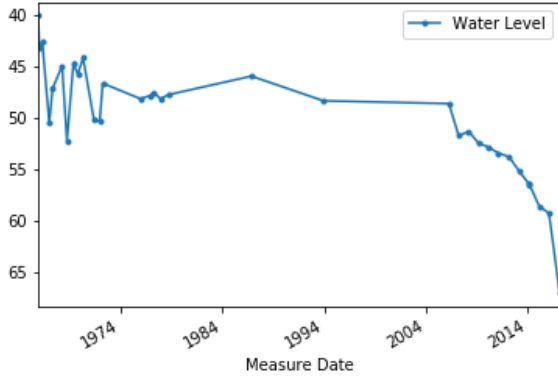
Close-up view of well locations (056 N17 E41 12DCCC1; 056 N17 E42 06BBCC1; 056 N17 E41 01BCBC1; 056 N18 E42 19CABB1), photograph locations (FIDs 5 and 6), and AOIs (FIDs 1 and 2).



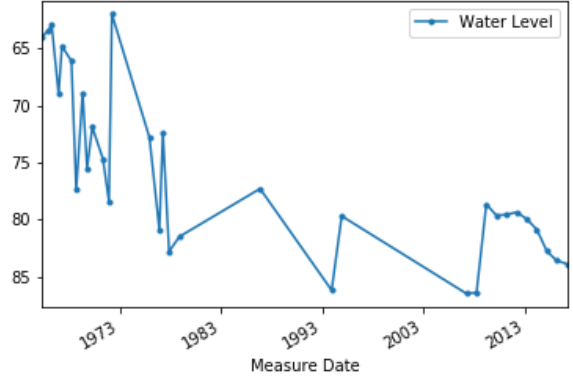
West facing photograph (pc_number 506; AOI FID 1).



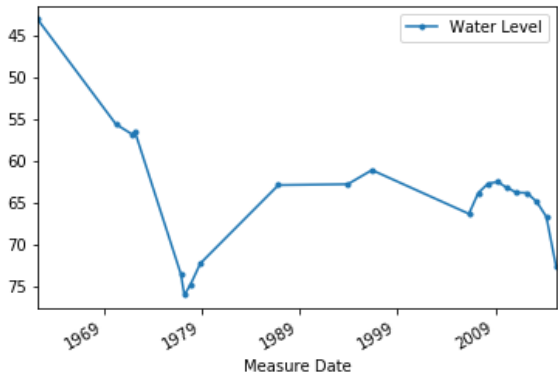
Northwest facing photograph (pc_number 492; AOI FID 2).



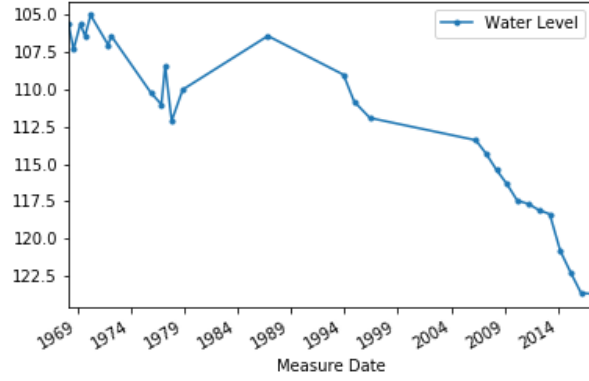
Well hydrograph (feet below surface): 056 N17 E42 06BCC1.



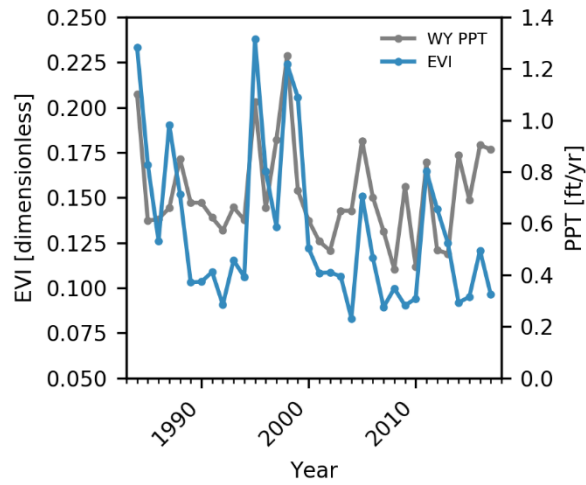
Well hydrograph (feet below surface): 056 N18 E42 19CABB1.



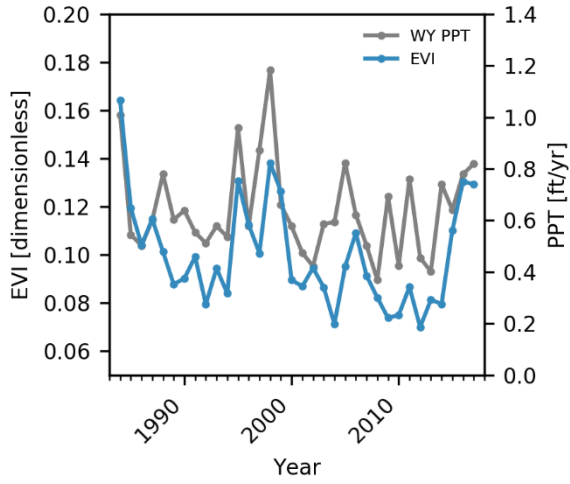
Well hydrograph (feet below surface): 056 N17 E41 12DCCC1.



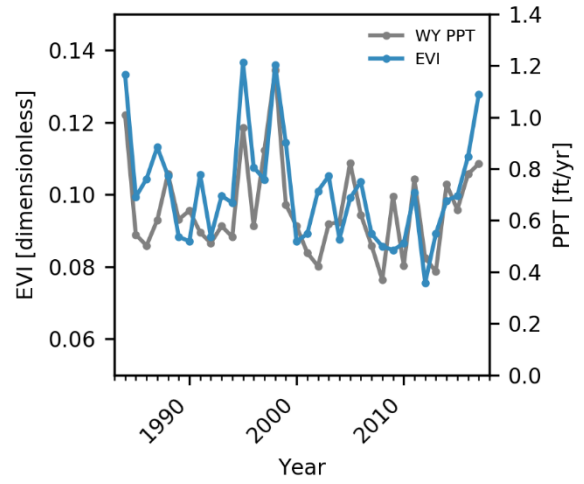
Well hydrograph (feet below surface): 056 N17 E41 01BCBC1.



EVI and PPT for AOI (FID 0).

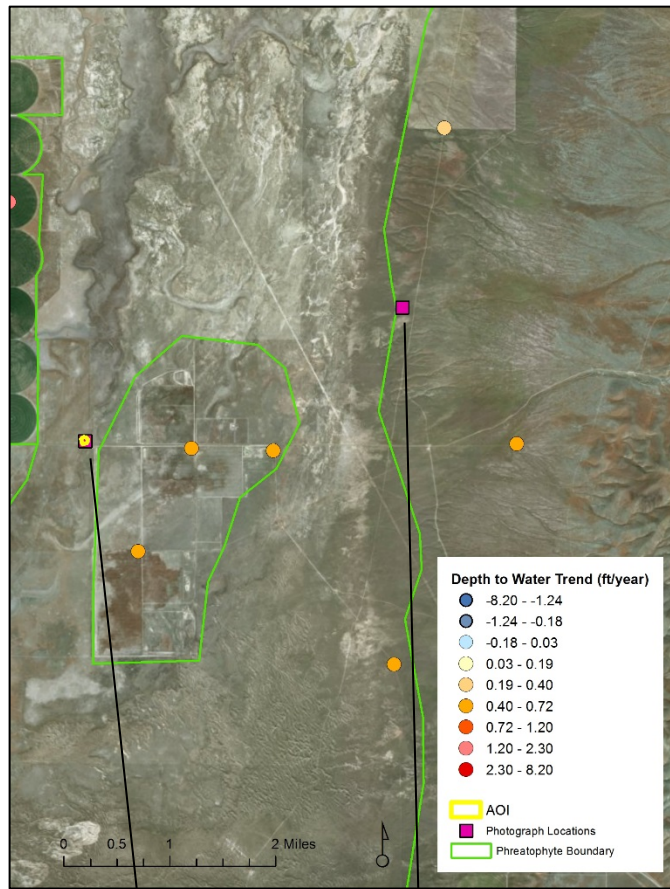


EVI and PPT for AOI (FID 1).



EVI and PPT for AOI (FID 2).

Appendix 1-9. Paradise Valley (HA 69) Close-up, Site Photographs, Well Hydrographs, and AOI EVI-PPT Graph for South-Eastern Part of the Valley



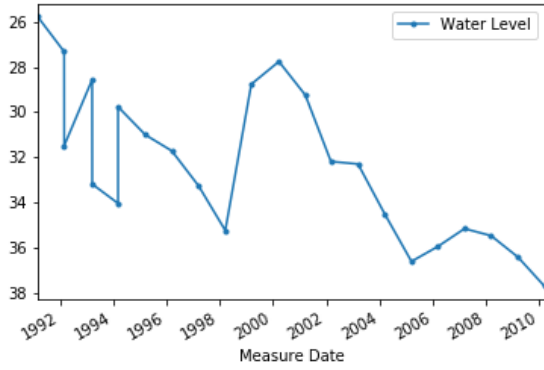
Close-up view of well locations (069 N38 E39 22ABAA1; 069 N39 E39 36CDCD1; 069 N38 E39 21AAA1; 069 N38 E39 28BAAA1), photograph locations (FIDs 0 and 1), and an AOI (FID 0).



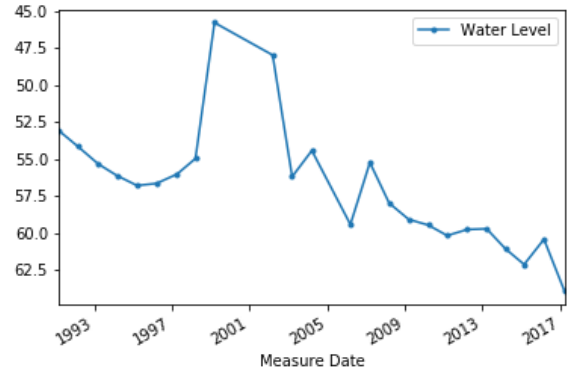
West facing photograph (pc_number 363; AOI FID 0).



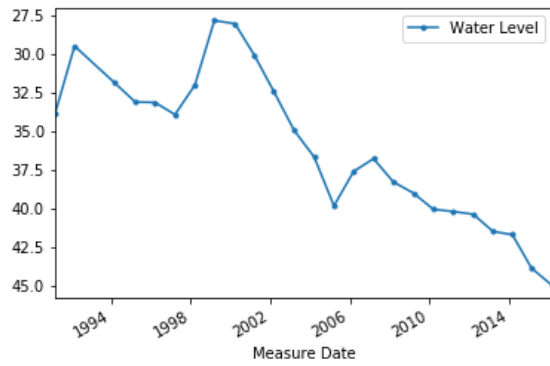
West facing photograph (pc_number 359).



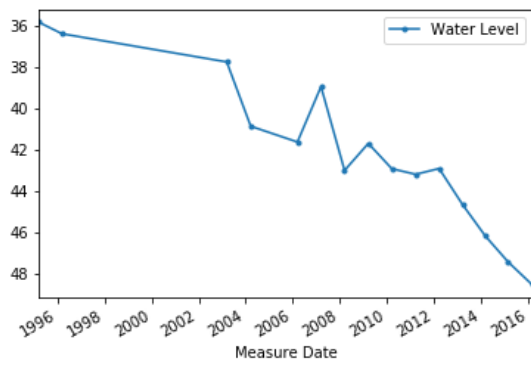
Well hydrograph (feet below surface): 069 N38 E39 22ABAA1.



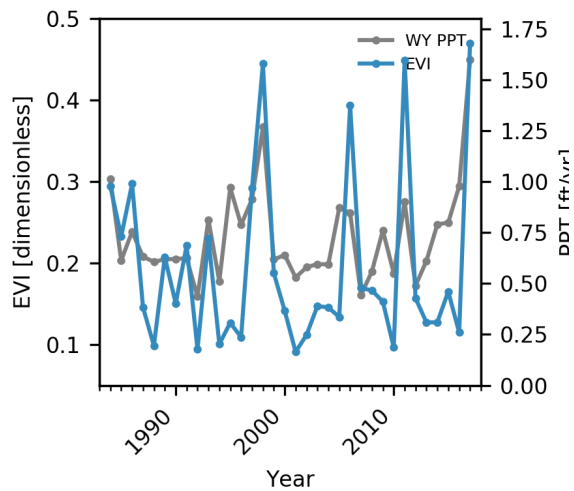
Well hydrograph (feet below surface): 069 N39 E39 36CDCD1.



Well hydrograph (feet below surface): 069 N38 E39 21AAA1.

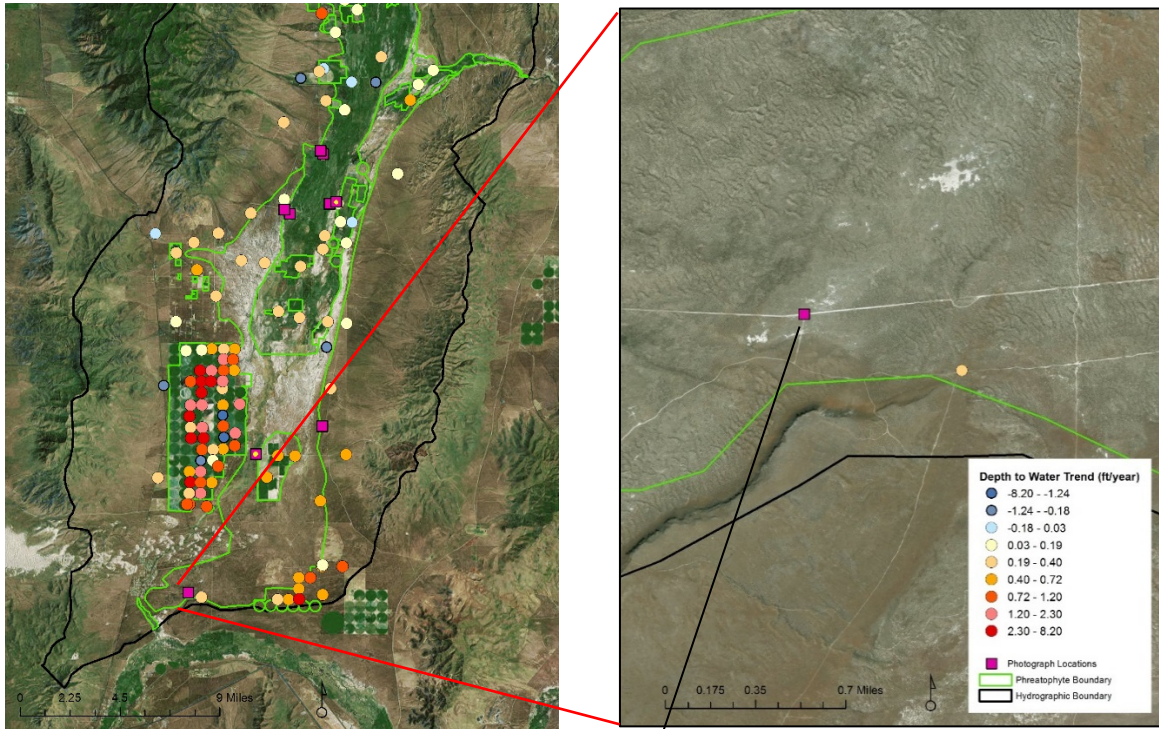


Well hydrograph (feet below surface): 069 N38 E39 28BAAA1.



EVI and PPT for AOI (FID 0).

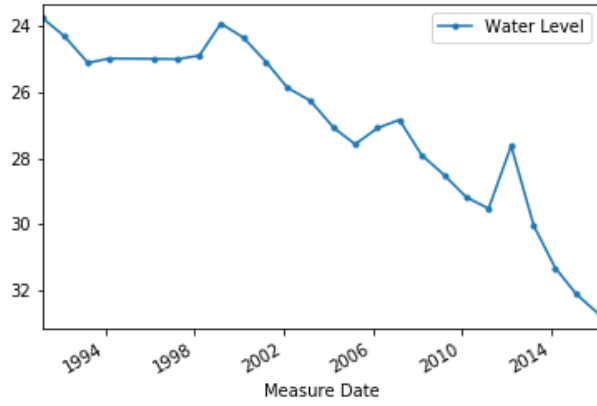
Appendix 1-10. Paradise Valley (HA 69) Close-up, Site Photographs, and Well Hydrograph for Southern Part of the Valley



Close-up view of well location (069 N37 E38 24ACC1) and photograph location (FID 8).

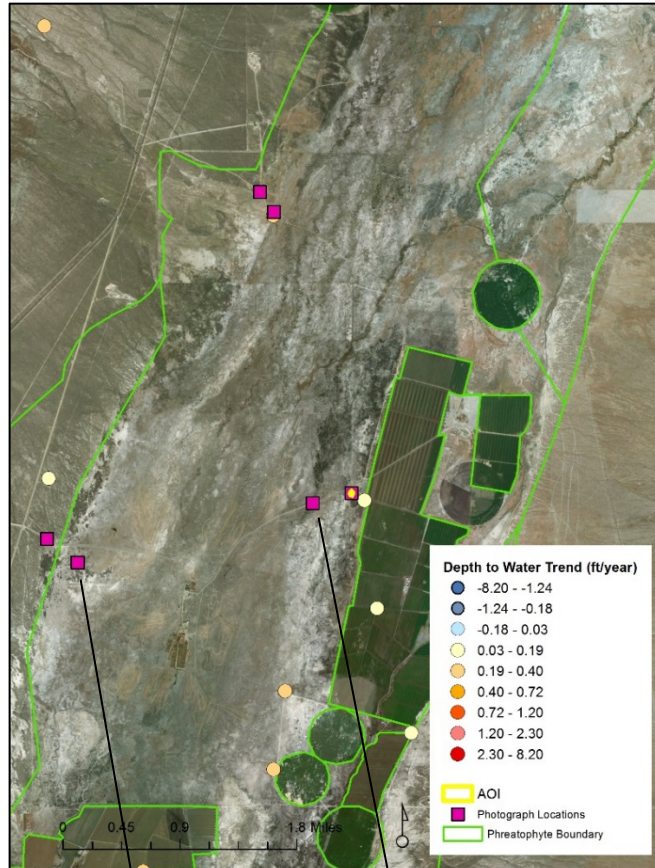


Northeast facing photograph (pc_number 416).



Well hydrograph (feet below surface): 069 N37 E38 24ACC1.

Appendix 1-11. Paradise Valley (HA 69) Close-up, Site Photographs, Well Hydrographs, and AOI EVI-PPT Graph for North-Central Part of the Valley



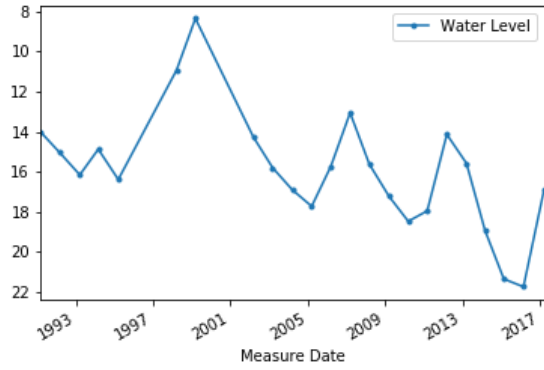
Close-up view of well locations (069 N39 E39 04BDC 1; 069 N40 E39 22CBAB1; 069 N40 E39 24CBDA1; 069 N40 E39 11ADDC1), photograph locations (FIDs 2-7), and an AOI (FID 1).



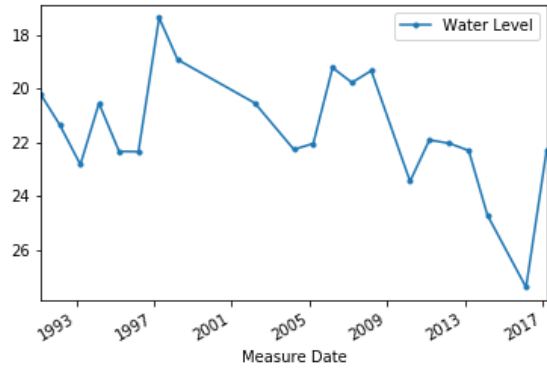
Southeast facing photograph (pc_number 384).



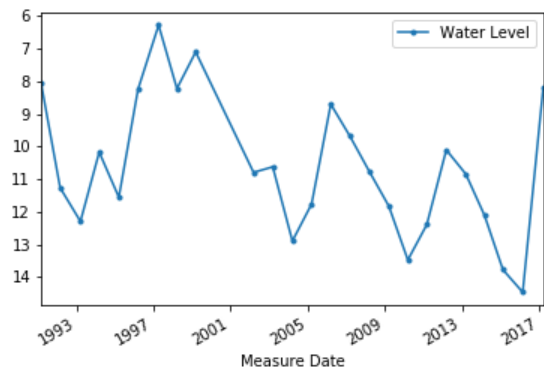
North facing photograph (pc_number 371).



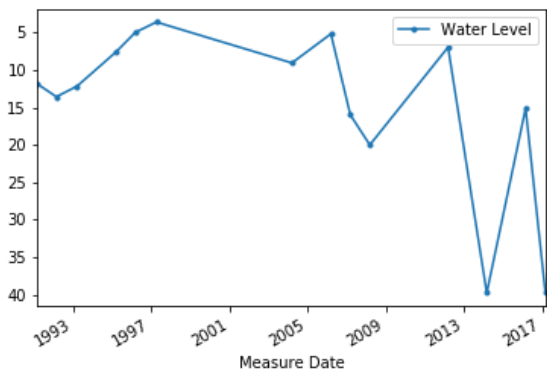
Well hydrograph (feet below surface): 069 N39 E39 04BDC 1.



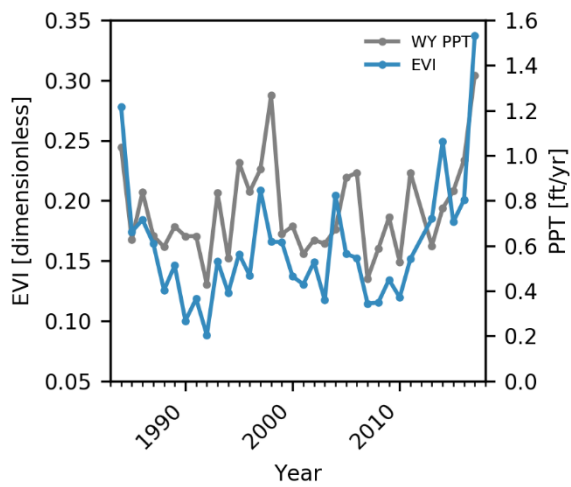
Well hydrograph (feet below surface): 069 N40 E39 22CBAB1.



Well hydrograph (feet below surface): 069 N40 E39 24CBDA1.

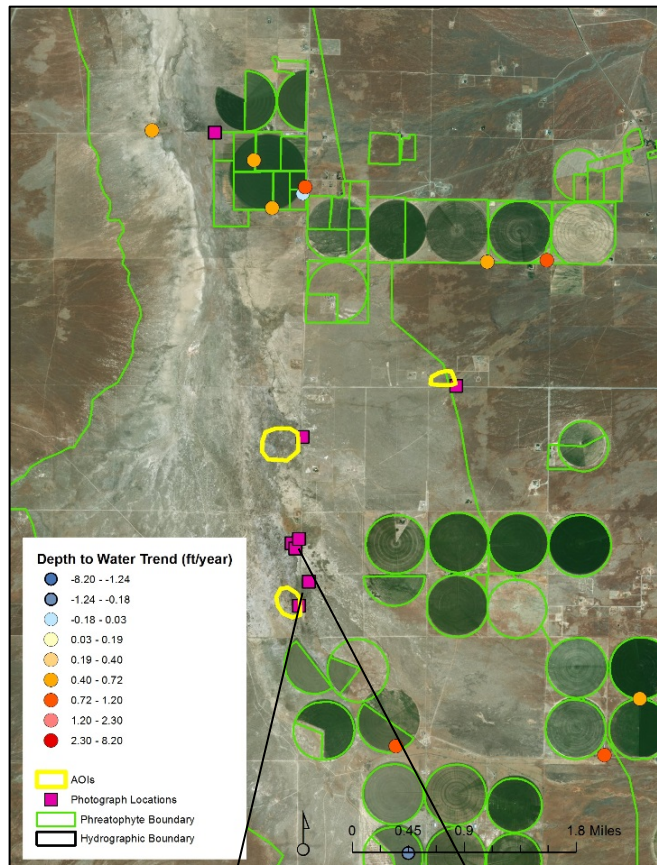


Well hydrograph (feet below surface): 069 N40 E39 11ADDC1.



EVI and PPT for AOI (FID 1).

Appendix 1-12. Grass Valley (HA 71) Close-up, Site Photographs, Well Hydrographs, and AOI EVI-PPT Graphs for Central Part of the Valley



Close-up view of well location (071 N33 E37 13DDCB1), photograph locations (FIDs 0-7), and AOIs (FIDs 1-3).



East facing photograph (pc_number 512; AOI FID 2).



West facing photograph (pc_number 514).



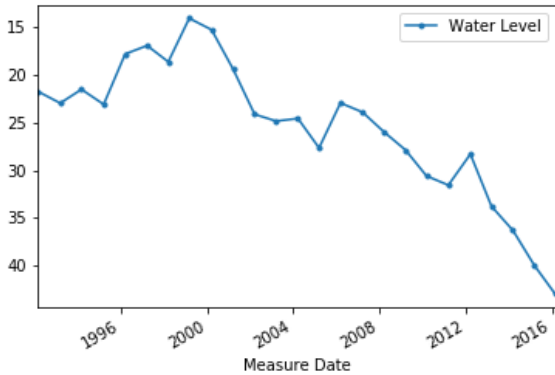
West facing photograph (pc_number 515).



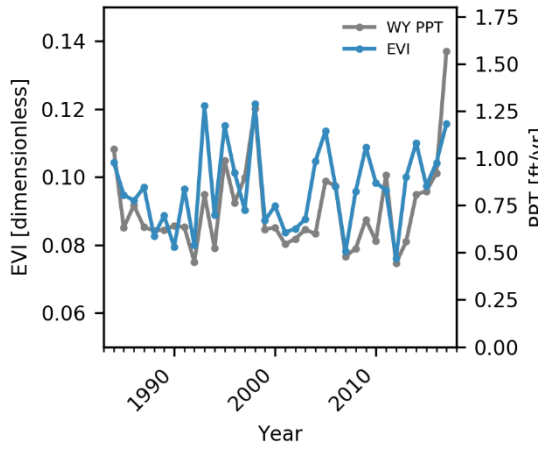
West facing photograph (pc_number 518; AOI FID 3).



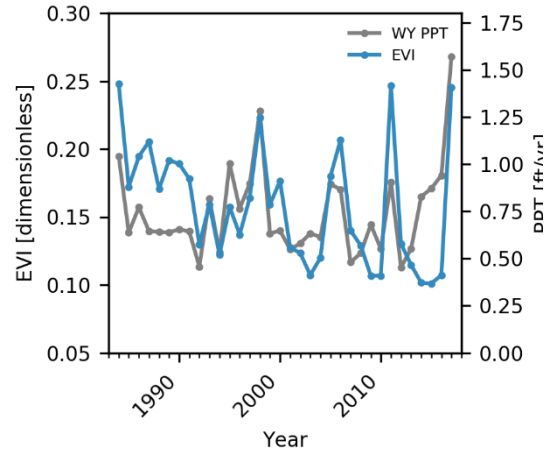
North facing photograph (pc_number 520; AOI FID 1).



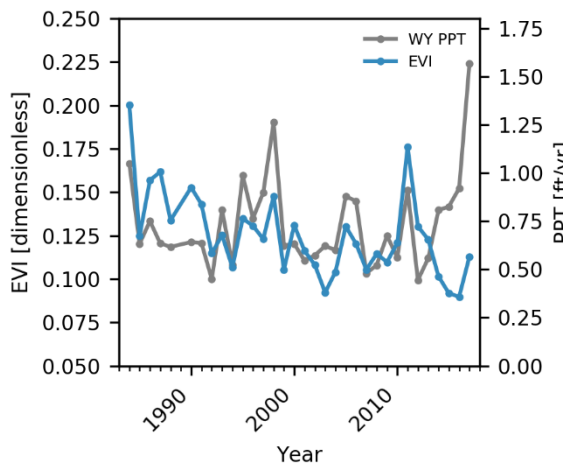
Well hydrograph (feet below surface): 071 N33 E37 13DDCB1.



EVI and PPT for AOI (FID 1).

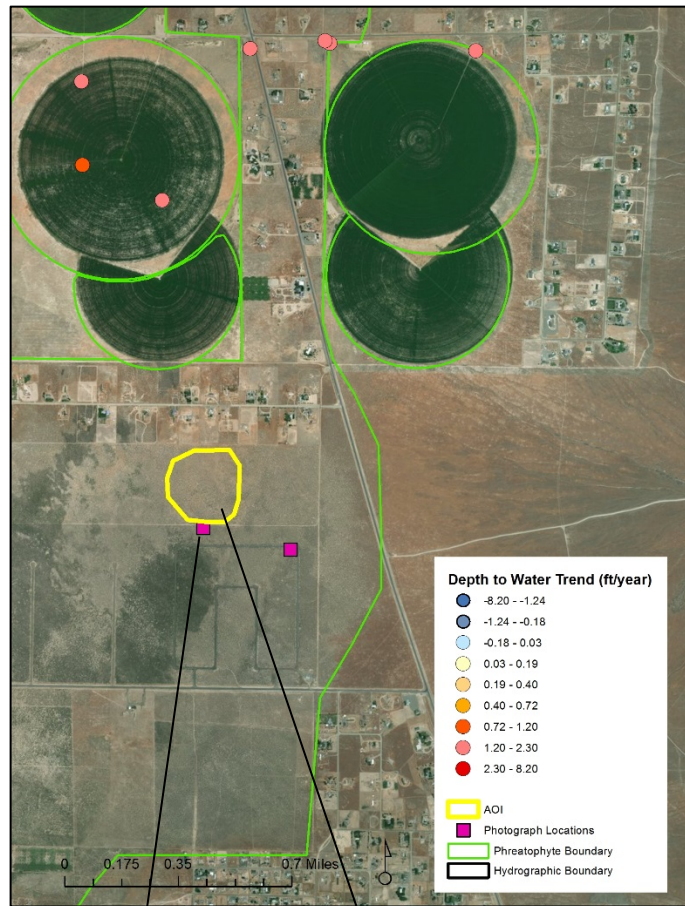


EVI and PPT for AOI (FID 2).



EVI and PPT for AOI (FID 3).

Appendix 1-13. Grass Valley (HA 71) Close-up, Site Photographs, Well Hydrographs, and AOI EVI-PPT Graph for Northern Part of the Valley



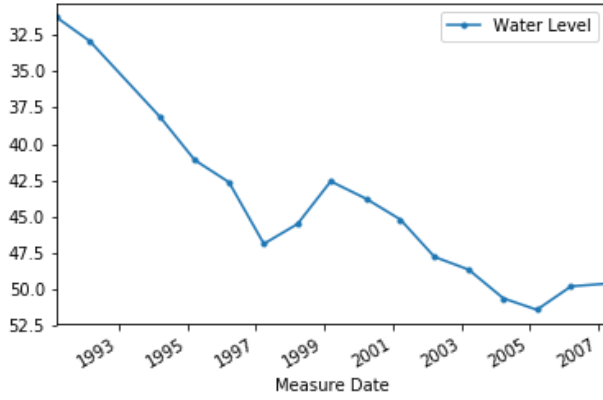
Close-up view of well location (071 N35 E37 36BDCB1), photograph locations (FIDs 8 and 9), and an AOI (FID 0).



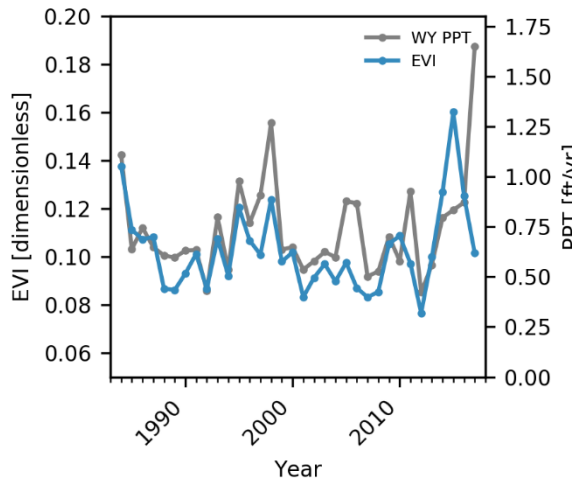
West facing photograph (pc_number 548; AOI FID 0).



North facing photograph (pc_number 553; AOI FID 0).

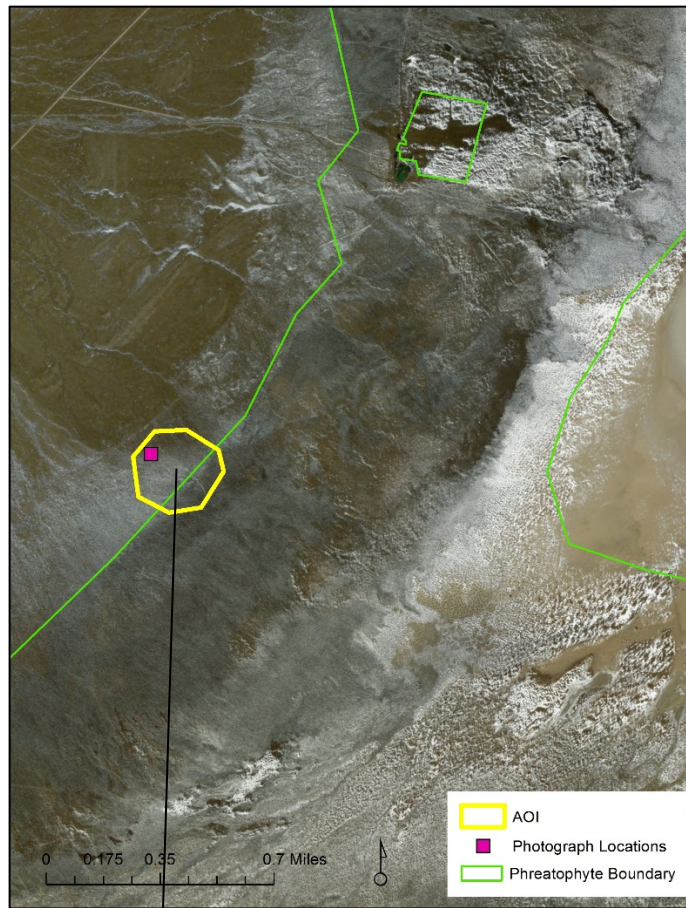


Well hydrograph (feet below surface): 071 N35 E37 36BDCB1.



EVI and PPT for AOI (FID 0).

Appendix 1-14. Edwards Creek Valley (HA 71) Close-up, Site Photographs, and AOI EVI-PPT Graph for West-Central Part of the Valley



Close-up view of photograph location (FID 0) and an AOI (FID 0).

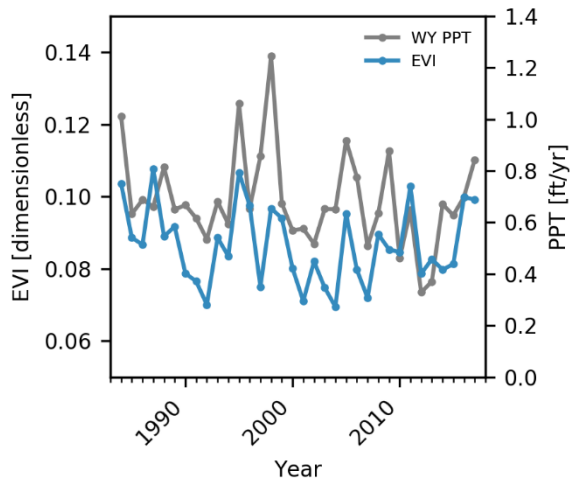


West facing photograph (pc_number 420; AOI FID 0).



East facing photograph (pc_number 425; AOI FID 0).

West facing photograph (pc_number 428; AOI FID 0).



EVI and PPT for AOI (FID 0).

APPENDIX 2 - Database Documentation

The following text outlines the database source information, documentation, and file structure. The database contains spatial data and hydrology data gathered/prepared in 2017 for groundwater dependent ecosystems in six hydrographic areas (HA) of Nevada. HAs within the database include:

HA 30A- Kings River Valley

HA 33A- Quinn River Valley

HA 56- Upper Reese River Valley

HA 69- Paradise Valley

HA 71- Grass Valley

HA 133- Edwards Creek Valley

Each HA has its own folder with six subfolders (HA 133 Edwards Creek Valley only has five since there are no water level measurements in the basin) and two geographic information system (GIS) map exchange documents (.mxd), ArcMap versions 10.3 and 10.4. Data layers within the ArcMap documents come from the subfolders for each basin. The six subfolders within each HA folder include: `evi_trend`, `groundwater_level_data`, `HA_boundary`, `photo_locations`, `phreatophyte_boundary`, and `zonal_photo_site_stats`.

The `evi_trend` subfolder contains three rasters (TIFF images), one that represents the long-term (1984-2017) trends in the enhanced vegetation index (EVI) determined by the Theil-Sen slope estimator, another that shows the Mann-Kendall p-value significance (.10 level) of those EVI trends, and a third that shows the trends that are statistically significant (.10 level). The Theil-Sen slope estimator determines the slope as the median of all slopes between paired values. More information about the Theil-Sen slope estimator and Mann-Kendall p-value can be found at the following links:

<https://docs.scipy.org/doc/scipy-0.15.1/reference/generated/scipy.stats.mstats.theilslopes.html>

<https://docs.scipy.org/doc/scipy-0.15.1/reference/generated/scipy.stats.kendalltau.html>

For the EVI trend map, red colors indicate areas where EVI trends are decreasing, whereas blue colors indicate areas where EVI trends are increasing. Yellow/tan colors indicate areas with little to no EVI trends. For the p-value map, black indicates that the EVI trend is significant at the .10 level, and white indicates that the EVI trend is not significant at the .10 level.

The `groundwater_level_data` subfolder contains the spatial locations of wells and the median Theil-Sen slope of water level trends in a shapefile format (`NV_DWR_Wells.shp`), hydrographs of all water level measurements for each well, and three excel files containing more information about the wells. The first excel file (`SiteData.xls`) contains information about the wells. Columns included are Site Name, USGS Site ID, Status, Well Name, Owner, Well Depth, Permit No., Well Log, Township, Range, Section, Qtr Sec, Latitude, Longitude, Elevation, Basin Name, and remarks that were made about the well. The second

excel file (WaterLevelData.xls) contains water level measurement information from each well. Columns include the Site Name, Measurement Date, Water Level (depth to water in feet), Status, Method, and remarks. The third excel file (WellLocations_out.csv) contains the same information as the first excel file (SiteData.xls), but also includes the median Theil-Sen slope of trends and the Mann-Kendall p-value associated with the trends. Additional columns in this file include WL_min, WL_max, WL_STD, WL_mean, WL_median, Num_Obs, median, lower, upper, Kendall_tau, and MK_p_value. The WL_min, WL_max, WL_STD, WL_mean, and WL_median represent the minimum, maximum, standard deviation, mean and median of water levels for each well, respectively. Num_Obs represents the number of measurements that were taken at each well. Median, lower, and upper columns are the median, upper 90% confidence level, and lower 90% confidence level of Theil-Sen slopes. The Kendall_tau column is the Kendall Tau value used for trend analysis. The MK_p_value is the p-value associated with water level trends calculated using the Kendall Tau value.

The HA_boundary subfolder contains a single shapefile representing the extent of the HA defined by the Nevada State Engineer and the State of Nevada Division of Water Resources. The shapefile's spatial reference is NAD 83 UTM zone 11. The attribute table of the shapefile contains information about the HA. Important columns to note include HYD_AREA, HYD_AREA_N, SUBAREA_NA, HYD_REGION, and HYD_REGI_1. The HYD_AREA column represents the number of the HA. The HYD_AREA_N column represents the name of the HA. The SUBAREA_NA column represents the sub areas of the HA if they exist. The HYD_REGION column represents the number of the larger hydrographic region that the HA belongs to. The HYD_REGI_1 column represents the name of the larger hydrographic region that the HA belongs to.

The photo_locations subfolder contains a single shapefile (e.g. HA56_photos.shp) of the locations where photographs were taken in the field during the summer of 2017 and another folder (photos) containing the actual photographs as JPEGs. The attribute table of the shapefile in the photo_locations subfolder contains information that was recorded during the acquisition of photographs. Columns include Date, Photos, pc_number, Hyperlink, Comments, GW_depth, and Camera_number. The Date column represents the day that photographs were taken from respective locations. The Photos column corresponds to the folder names where photographs are stored and are described in the next section of this document. The pc_number column represents the unique JPEG number that each photograph is stored as in the folders. The Hyperlink column contains a direct link to a Google Doc where photographs are also stored and can be viewed using the ArcMap mxd. The Comments column contains brief summaries of qualitative vegetation assessments from photograph locations. They also include information about the direction that the photograph was taken. The GW_depth column contains general information about the depth to groundwater near the photograph locations obtained from the Nevada Division of Water Resources'(NDWR) Nevada Hydrology online database. The Camera_number column represents the number of each photograph that is recorded on the actual camera that was used. These numbers differ from the JPEGs described in the forthcoming section.

Photographs are separated and stored in unique folders that describe which trip, location, basin, and region of the basin they were taken at. The structure of the photograph folders, for example, are T1_Loc1_basin_name_and_region. T# represents the trip number, Loc# represents the location the photograph was taken at, and basin_name_and_region represents the HA and regions of the HA where the photographs were taken. The folders that store the JPEGs and the JPEGs themselves correspond to the 'Photos' and 'pc_number' columns, respectively, from the attribute table of the photos shapefile.

The phreatophyte_boundary subfolder contains a single shapefile of Area of Interest (AOI) polygon features representing the spatial extent of phreatophyte vegetation. This may also be considered as the area of potential groundwater discharge. The attribute table of the shapefile contains information about how the boundaries were obtained and what the different ET units (i.e. vegetation types) are. Columns included are Type, Source, Comments, Area, HYD_AREA, and HYD_AREA_N. The Type column describes the ET unit that is assigned to each polygon; these can include phreatophytes (shrublands), meadow, riparian, and irrigated croplands. The Source column represents the data source where original phreatophyte boundaries were obtained and modified from; these came from numerous sources including Reconnaissance Series Reports, Water Resource Bulletins, and another groundwater study by the USGS (sources included at the end of this section). The Comments column contains information about what data sets were used to modify the original boundaries; data sets used for modifications included Landsat 8 Thermal Infrared Sensor (TIRS) data, National Agriculture Imagery Program (NAIP) data, Normalized Difference Vegetation Index (NDVI) data, and Digital Elevation Models (DEM). The Area column represents the area of each polygon within the shapefile (acres). The HYD_AREA column contains the number of the HA and subarea number. The HYD_AREA_N column contains the name of the HA.

Reconnaissance Series Reports and Water Resource Bulletins:

<http://water.nv.gov/reconreports.aspx>; <http://water.nv.gov/bulletins.aspx>

Water budget estimates for 14 HAs in the middle Humboldt River basin, north-central Nevada: <https://pubs.er.usgs.gov/publication/wri004168>

The zonal_photo_site_stats subfolder contains zonal stats that were calculated using a method outlined in Beamer et al. (2013). There is a figures folder, locations folder, and three excel files relating to zonal stats for areas where photographs were taken. The figures folder contains numerous graphs comparing the water year actual evapotranspiration (ET), groundwater evapotranspiration (ETg), water year reference/potential evapotranspiration (ETo), water year precipitation (PPT), and EVI for every polygon that was used for calculating zonal stats. Gridded PPT and ETo from the University of Idaho's Gridded Surface Meteorological Data (UofI METDATA) was used in the zonal stats analysis. The locations folder contains a shapefile of polygons that were used for calculating zonal stats. The attribute table of this shapefile contains information about the location, area, and corresponding photograph number. The location column describes which HA the polygon

lies within and the region of the HA it is in. The Area column represents the acreage of the polygon. The JPEG column represents the number of the photograph that corresponds to the area where zonal stats were calculated.

The first excel file (.csv) is a table containing the zonal stats that were calculated for each AOI polygon. Units of the excel file are millimeters. Polygons are separated by the FID number from the attribute table of the shapefile. Columns include ZONE_NAME, ZONE_FID, Date, SCENE_ID, PLATFORM, PATH, ROW, YEAR, MONTH, DAY, DOY, PIXEL_COUNT, PIXEL_TOTAL, FMASK_COUNT, FMASK_TOTAL, FMASK_PCT, ETSTAR_COUNT, CLOUD_SCORE, QA, NDVI_TOA, NDWI_TOA, ALBEDO_SUR, TS, EVI_SUR, ETSTAR_MEAN, ETG_MEAN, ETG_LPI, ETG_UPI, ET_MEAN, ET_LPI, ET_UPI, ET_LCI, ET_UCI, WY_ETO, and WY_PPT. The ZONE_NAME and ZONE_FID columns correspond to the FID of the polygon. The DATE column is the data in which the satellite acquired the image. The SCENE_ID column summarizes image acquisition information. The PLATFORM column contains the abbreviated name of the satellite. The PATH column represents the vertical region the image captures. The Row represents the horizontal region the image captures. YEAR, MONTH, DAY, and DOY pertain to the timing of image acquisition. PIXEL_COUNT represents the number of pixels (30m x 30m) used in zonal stats calculations. PIXEL_TOTAL is the amount of pixels that are within or touch the polygons. FMASK_COUNT is the amount of pixels that were cloud masked. FMASK_TOTAL is the same as PIXEL_TOTAL. FMASK_PCT is the percentage of pixels that were cloud masked. ETSTAR_COUNT is amount of pixels that did not have enough vegetation signal. CLOUD_SCORE is a dimensionless number describing how much cloud contamination is present in the image. The QA column can be disregarded. NDVI_TOA is the top of atmosphere NDVI value. NDWI_TOA is the top of atmosphere normalized difference water index. ALBEDO_SUR is the albedo of the surface for the polygon. TS is the land surface temperature of the polygon. EVI_SUR is the mean EVI of the polygon calculated from each image. ETSTAR_MEAN is the mean ET star calculated from EVI_SUR using the Beamer method. ETG_MEAN is the mean ETg. ETG_LPI is the lower 90% prediction interval ETg estimate. ETG_UPI is the upper 90% prediction interval ETg estimate. ETG_LCI is the lower 90% confidence interval ETg estimate. ETG_UCI is the upper 90% confidence interval ETg estimate. ET_MEAN is the mean actual ET. ET_LPI is the lower 90% prediction interval ET estimate. ET_UPI is the upper 90% prediction interval ET estimate. ET_LCI is the lower 90% prediction interval ET estimate. ET_UCI is the upper 90% prediction interval ET estimate. WY_ETO is the water year reference/potential ET. WY_PPT is the water year precipitation. The second and third excel files (annual.xls and daily.xls) are summary tables of the annual and daily zonal Stats for each AOI. The units of the second excel file (annual.xls) are feet, whereas the units of the third excel file are millimeters. Their column headers are similar to the ones previously mentioned in the first excel file, however, the annual summary table has a few columns with the minimum, maximum, median, and mean EVI. The annual summary table values match the annual values in the graphs from the figures folder.

The ArcMap documents within each HA's folder contain the data sets that have previously been mentioned. These documents are helpful for viewing the spatial characteristics of each data set and have important information in the attribute tables. The organization of these ArcMap documents are as follows (e.g. HA 30A Kings River Valley):

NV_DWR_Wells_HA30A (shapefile); Alias = "Depth to Water Trend (ft/year)" - This shapefile comes from the groundwater_level_data subfolder. Values displayed represent the median trend in water levels as calculated from Theil-Sen slope estimator. Graduated symbology is used to illustrate differences in water level trends. Big, red circles represent wells where large decreases in water levels are occurring. Small, blue circles represent wells where increases in water levels are occurring.

HA30A_photos (shapefile); Alias = "Photograph Locations" - This shapefile comes from the photo_locations subfolder. Pink/purple squares represent the locations where photographs were taken and vegetation assessments were conducted. Supplemental information is in the attribute table and so are the hyperlinks to photographs.

HA30A_zonal_photo_stats (shapefile); Alias = "AOIs" - This shapefile comes from the zonal_photo_site_stats subfolder. These polygons (outlined in a thin, blue line) represent the areas used in zonal stats calculations. Their extent corresponds to the area photographed and recorded. The JPEG numbers that each polygon relates to is in the attribute table.

HA30A_phreatophytes (shapefile); Alias = "Phreatophyte Boundary" - This shapefile comes from the phreatophyte_boundary subfolder. These polygons (outlined in green) represent the areas of phreatophyte shrublands, meadows, riparian, and irrigated areas. Supplemental information about how they were obtained and modified is in the attribute table.

HA30A_nad83utm11 (shapefile); Alias = "Hydrographic Boundary" - This shapefile comes from the HA_boundary subfolder. The polygon (outlined in black) represents the boundary of the HA. Supplemental information is in the attribute table.

sigtren_2017 (raster); Alias = "Significant EVI Trend" - This raster comes from the evi_trend subfolder. The red color indicates areas where EVI trends are decreasing. The blue color indicates areas where EVI trends are increasing. The yellow/tan color indicates areas with little or no EVI trends. Date range is 1984-2017 (inclusive). This raster has been masked so that only pixel values with a p-value lower than 0.1 are included.

trend_2017 (raster); Alias = "EVI Trend" - This raster comes from the evi_trend subfolder. The red color indicates areas where EVI trends are decreasing. The blue color indicates areas where EVI trends are increasing. The yellow/tan color indicates areas with little or no EVI trends.

p_value_2017 (raster); Alias = "p_val_2017" - This raster comes from the evi_trend subfolder. The black indicates areas where EVI trends are significant at the .10 level. The white indicates areas where EVI trends are not significant at the 0.10 level.

APPENDIX 3 – Summary Table of Results from Water Level, EVI, and PPT Trend Analyses and Field Investigations

Appendix	HA	Well #	Yrs ¹	WT drop (ft) ^{2,8}	WT signif ³	EVI signif ⁴	G ⁵	R ⁶	S ⁷
1-1	30A	030A N45 E34 29ABBC1	1998-2016	50	Y	N	P	--	PS
1-1	30A	030A N45 E34 29ABBC2	1998-2016	15	Y	N	P	--	PS
1-2	30A	030A N44 E34 16AAAA1	1994-2016	30	Y	N	P	--	PSM
1-3	33A	033A N44 E36 26ACB1	2012-2017	-10	N	Y	P	PS	--
1-3	33A	033A N44 E36 22DCAA1	2006-2016	5	N	N	P	PS	--
1-3	33A	033A N44 E36 34ADBC1	2012-2017	5	Y	N	P	PS	--
1-4	33A	033A N44 E36 33BCDA1	2006-2016	3.5	Y	Y	P	--	PSM
1-4	33A	033A N43 E36 04DDDD1	1992-2017	7	Y	N	P	--	PSM
1-5	33A	033A N43 E36 14BCBB1	2006-2017	8	Y	N	--	--	--
1-5	33A	033A N42 E36 08AAB1	1996-2017	8	Y	N	--	--	--
1-5	33A	033A N41 E36 06ABBB1	1995-2016	10	Y	Y	--	--	--
1-5	33A	033A N41 E36 06CBAA1	1996-2017	8	Y	N	--	--	--
1-8	56A	056 N17 E42 06BBCC1	1965-2017	20	Y	Y		PSM	PSM
1-8	56A	056 N18 E42 19CABB1	1965-2017	20	Y	N	P	P	--
1-8	56A	056 N17 E41 12DCCC1	1965-2017	30	Y	Y	--	PSM	PSM
1-8	56A	056 N17 E41 01BCBC1	1965-2017	17	Y	Y	--	PSM	PSM
1-9	69A	069 N38 E39 22ABAA1	1991-2011	12	Y	Y	P	PSM	PSM
1-9	69A	069 N39 E39 36CDCD1	1991-2017	10	Y	N	P	P	P
1-9	69A	069 N38 E39 21AAA1	1991-2017	15	Y	Y	--	PSM	PSM
1-9	69A	069 N38 E39 28BAAA1	1995-2017	12	Y	Y	--	PSM	PSM
1-10	69A	069 N37 E38 24ACC1	1991-2017	8	Y	N	P	--	PS
1-11	69A	069 N39 E39 04BDC 1	1991-2017	8	Y	Y	P	--	PS
1-11	69A	069 N40 E39 22CBAB1	1991-2017	6	N	Y	P	--	PS
1-11	69A	069 N40 E39 24CBDA1	1991-2017	6	Y	Y	PS	--	--
1-11	69A	069 N40 E39 11ADDC1	1991-2017	30	N	Y	P	--	--
1-12	71A	071 N33 E37 13DDCB1	1992-2017	20	Y	Y	P	PS	--
1-13	71A	071 N35 E37 36BDCB1	1991-2007	20	Y	N	PSM	P	P

¹Years of observations at each well

²Feet of water table decline over the years of observations

³Y if water table decline is significant at p = 0.10, N if water table decline is not significant

⁴Y if trend in EVI is significant at p = 0.10, N if trend in EVI is not significant

⁵G = greasewood; P if it is present; S if stress is observed; M if mortality is observed

⁶R = rabbitbrush; P if it is present; S if stress is observed; M if mortality is observed

⁷S = sagebrush; P if it is present; S if stress is observed; M if mortality is observed

⁸Negative values indicate an increase in water level at the well